Journal of Hydrology 665 (2026) 134690

Contents lists available at ScienceDirect

Journal of Hydrology

journal homepage: www.elsevier.com/locate/jhydrol

Robust multi-objective optimization with multi-scenario coupling: Spatial equilibrium-based water resources allocation in the upper and middle reaches of the Huaihe River Basin

Jitao Zhang [a,*], Jinyu Meng [b], Zengchuan Dong [b], Dimitri Solomatine [c,d,e], Hui Xu [a], Wenzhuo Wang [b], Daoli Wang [b], Tianyan Zhang [b], Guang Yang [f]

[a] College of Agricultural Science and Engineering, Hohai University, Nanjing 210098, China
[b] College of Hydrology and Water Resources, Hohai University, Nanjing 210098, China
[c] Water Resources Section, Delft University of Technology, 2628 CD Delft, the Netherlands
[d] IHE Delft Institute for Water Education, 2628 AX Delft, the Netherlands
[e] Water Problems Institute of RAS, 119333 Moscow, Russia
[f] Nanjing Hydraulic Research Institute, Nanjing 210029, China

ARTICLE INFO

This manuscript was handled by Andras Bardossy, Editor-in-Chief

Keywords:
Water resource allocation
Uncertainties
Spatial equilibrium
Robustness
Copula Function
Wet and dry encounters

ABSTRACT

Optimized water resource allocation is critical for promoting sustainable regional development. However, the intensification of climate change impacts has increased the variability of water availability, thereby compounding uncertainty and complexity in water allocation decision-making. Meanwhile, mismatches in the spatial distribution of water supply and demand have also become an essential constraint to effectiveness and fairness of water allocation. Prior studies show weak correspondence between modeling frameworks to real world conditions and insufficiently describe regional balance, as well as the dynamic interaction between water inflow and demand under varying hydrological regimes. To address these challenges, this study develops a multi-objective water resource allocation model guided by spatial equilibrium principles, ensuring not only fair inter-regional allocation but also balanced co-development among water, socio-economic, and ecological subsystems. Regional balance is quantified with the Gini coefficient. Subsystem co-development is enforced via the coupling coordination degree. To address uncertainty, a nested multi-scenario robust optimization framework is proposed. It applies copula function to generate realistic encounter scenarios and applies a multi-objective probabilistic robustness evaluation to test solution stability and adaptability across scenarios. Applied to the upper and middle reaches of the Huaihe River Basin (HRB), the approach reduces the water-deficit rate by 45.42 % under extreme dry scenarios, lifts the coordination index to > 0.75, and increases reliability by 45.3 % compared with a traditional robust optimization baseline, demonstrating effectively optimize complex water resource systems while keeping both fairness and stability. This research offers a theoretical and practical framework for optimizing water resource allocation in complex and uncertain environments, contributing to the advancement of resilient and equitable water governance.

1. Introduction

Water resources are a fundamental natural element for the survival and development of human society. Its importance has become increasingly prominent amid continuous population growth and economic expansion (Li et al., 2023; O'Connell, 2017; Zhu et al., 2022). The demand for water resources is rising, and the conflict between supply and demand is becoming increasingly acute (Naderi et al., 2021). At the same time, the intensification of global climate change, especially the faster-than-expected rise in temperature, further disrupts the spatial and temporal patterns of precipitation and significantly increases the risk of water scarcity, and these trends not only exacerbate the pressure on the resource but also increase the systematic uncertainty facing water resources management (Meraj and Hashimoto, 2025). Under such uncertainty, proposing a water resources allocation model that is close to reality and takes into account equity, efficiency, and spatial balance has

* Corresponding author.
E-mail address: jitaozhang_hohai@hhu.edu.cn (J. Zhang).

https://doi.org/10.1016/j.jhydrol.2025.134690
Received 23 May 2025; Received in revised form 23 November 2025; Accepted 26 November 2025
Available online 27 November 2025

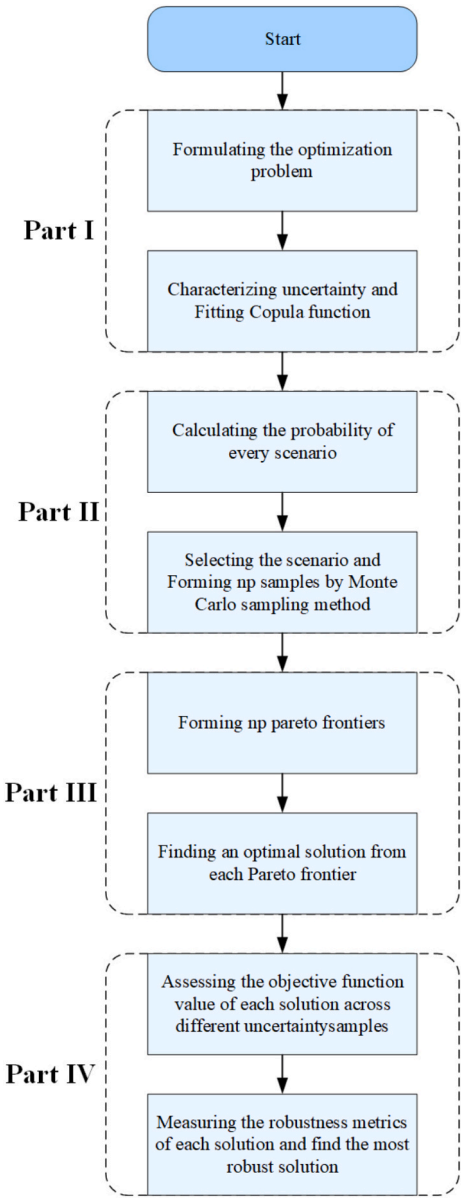

Fig. 1. Flowchart of the RMOMC algorithm.

become an important research frontier in global water resources management.

The theoretical study of optimal allocation of water resources, as a core issue of basin water resources management, began with the optimization model of reservoir scheduling proposed by Masse in 1946 (Lu et al., 2013). Since then, classical optimization methods represented by dynamic programming (Davidsen et al., 2015; Unami et al., 2019) and linear programming (Gorelick and Zheng, 2015) have been gradually formed, which provided a solid quantitative foundation for early water resource allocation.

In the mid-to-late 20th century, the introduction of system theory and large-scale system decomposition and coordination methods promoted the rapid development of multilevel and multi-objective water resources system modeling at regional and basin scales. Typical methods, such as goal-based planning (Li et al., 2018); analytic hierarchy process (Sun et al., 2016; Wang et al., 2022), and dynamic stepwise planning (Vališ et al., 2020), are widely used in complex scenarios such as multi-reservoir joint scheduling and integrated regional allocation.

With the improvement of information technology and computing power, water resources optimization models have gradually integrated simulation and optimization tools to form complex system models that support large-scale data processing and multi-scenario prediction, and the optimization objectives have expanded from single water quantity control to multi-objective synergism of water quantity-water quality, resources-economy, etc. (Cai et al., 2003; Candido Laíse et al., 2022; Liu et al., 2021). Khabat Khosravi emphasized that water quality modeling in riverine systems is crucial for effective water resource management and pollution mitigation planning (Khosravi et al., 2025). The water quantity-water quality joint allocation model constructed by Afzal (Afzal et al., 1992) and the coupling model proposed by Dai et al (Dai and Labadie, 2001) are typical paths of resource-environment-economy synergistic optimization. Zepeng Zhang proposed a multi-objective agricultural water-resources production model that accounts for both economic and ecological benefits from the dual perspectives of government and farmers (Zhang et al., 2025). Pen Qi proposed a water allocation management model considering crop water demand process from the perspective of water-carbon-economy nexus (Qi et al., 2025).

In recent years, the introduction of intelligent algorithms such as genetic algorithms (Dai and Labadie, 2001; Chakraei et al., 2021; Kumar and Yadav, 2022), co-evolution (Pan et al., 2023; Zhang et al., 2024), and neural networks (Qu et al., 2024; Wu et al., 2023) has effectively improved the solution efficiency and model adaptability. Nevertheless, climate change and human activities have introduced increasingly complex uncertainty into key hydrological variables such as streamflow and water level (Wang et al., 2019). To mitigate the impacts on water resources management, some researchers employ machine learning approaches to forecast the variables (Kaya, 2025; Ji et al., 2025; Kaya, 2025), thereby reducing uncertainty induced disturbances. High-precision satellite observations have also been utilized to improve estimation accuracy; for example, Kaya employed ICESat-2 ATL13 data to assess the drying rate of inland water bodies (Küçükoğlu and Kaya, 2026). In parallel, mathematical programming techniques-including fuzzy programming (Zhang et al., 2022), interval optimization (Li et al., 2022), and robust optimization (Shuai et al., 2022; Yuan et al., 2023) have been widely applied to enhance the robustness and implement ability of the scheme under uncertainty. Furthermore, game theory and Pareto-based decision frameworks have provided theoretical foundations for coordinating multi-actor interests in cross-regional, cross-sectoral, and even transboundary water-sharing problems (Madani, 2010).

Despite the deepening of the above research, the current water allocation is still insufficient to cope with complex uncertainty conditions and achieve system resilience and allocation robustness, especially in climate change, where traditional models can hardly effectively capture the dynamic evolution of the system. At the same time, there are still obvious shortcomings in technology, data, and management capacity in different regions. There is an urgent need to build a system of water resources optimization methods that consider multiple sources of uncertainty and regional spatial equilibrium to achieve a more efficient, fairer, and sustainable path of resource allocation.

Based on existing literature, this study addresses two critical gaps: the insufficient consideration of interregional equity and the inadequate treatment of uncertainty in conventional allocation models. To address the limitations, a spatial equilibrium oriented allocation model is developed that remains reliable under changing climate conditions. The model evaluates the coordinated advancement of water resources, economic activity, and ecosystems through the Coupling Coordination Degree, while regional balance is quantified using the Gini coefficient. To characterize uncertain inflows, numerous combinations of wet and dry conditions are generated using the Copula Function-based approach (a standard statistical method for modeling joint distributions and co-occurrence probabilities) and the robustness is assessed through a probabilistic performance evaluation across scenarios. This framework enables the identification of allocation schemes that are both spatially equitable and consistently robust under uncertainty.

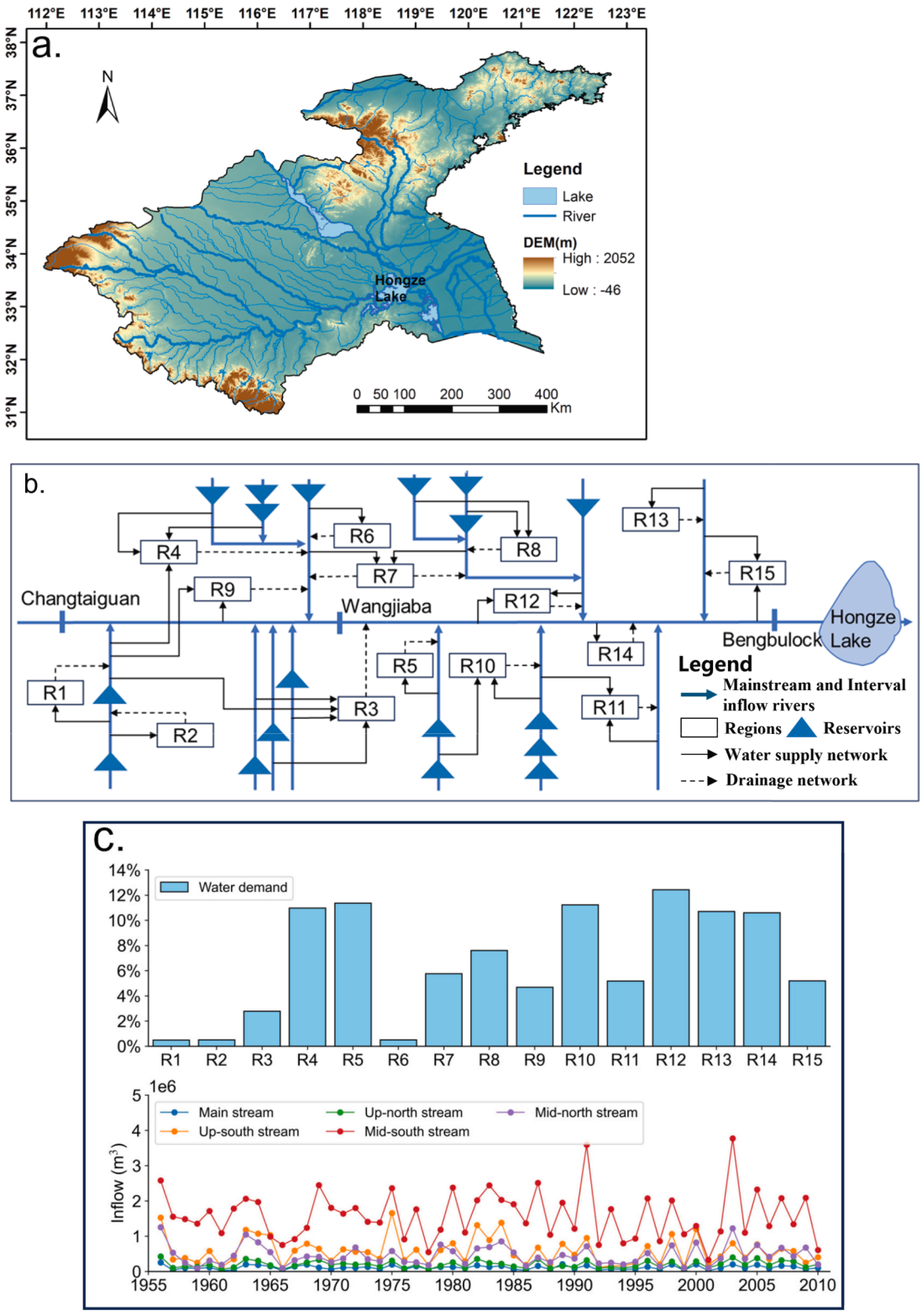

Fig. 2. Study area information (Fig. 2(a): Geographic information for the study area; Fig. 2(b): Schematic concept map of water allocation system; Fig. 2(c): Proportion of Water demand by water use units and Inflow volume in river basin).

2. Method

2.1. Robust multi-objective optimization with multi-scenario coupling

The Robust multi-objective optimization with multi-scenario coupling (RMOMC) algorithm is designed to systematically integrate multiple sources of uncertainty to improve the robustness of water resources management decisions. The method introduces the Copula function to characterize the dependency structure among uncertainty factors and generate diverse joint inflow scenarios to provide the probabilistic basis required for robustness evaluation. Building upon these scenarios, the RMOMC framework identifies solutions that satisfy

Table 1
Scenario probabilities of wet-dry encounters when the main stream is wet (All data are percentages).

Probability of wet-dry encounters		MW								
		C-WSW			C-WSP			C-WSD		
		C-W NW	C-W NP	C-W ND	C-W NW	C-W NP	C-W ND	C-W NW	C-W NP	C-W ND
W-B SW	W-B NW	**2.55 %**	0.93 %	0.20 %	1.28 %	0.40 %	0.00 %	0.53 %	0.20 %	0.00 %
	W-B NP	0.33 %	0.80 %	0.60 %	0.20 %	0.33 %	0.28 %	0.00 %	0.20 %	0.00 %
	W-B ND	0.00 %	0.28 %	1.68 %	0.00 %	0.00 %	0.53 %	0.00 %	0.08 %	0.00 %
W-B SP	W-B NW	0.28 %	0.13 %	0.00 %	0.53 %	0.20 %	0.08 %	0.80 %	0.28 %	0.00 %
	W-B NP	0.00 %	0.00 %	0.00 %	0.00 %	2.45 %	0.20 %	0.00 %	0.28 %	0.00 %
	W-B ND	0.00 %	0.00 %	0.60 %	0.00 %	0.00 %	0.60 %	0.00 %	0.08 %	0.48 %
W-B SD	W-B NW	0.00 %	0.00 %	0.00 %	0.20 %	0.00 %	0.00 %	1.60 %	0.48 %	0.00 %
	W-B NP	0.00 %	0.00 %	0.00 %	0.00 %	0.00 %	0.00 %	0.33 %	0.60 %	0.40 %
	W-B ND	0.00 %	0.00 %	0.28 %	0.00 %	0.00 %	0.53 %	0.00 %	0.28 %	2.03 %

Table 2
Scenario probabilities of wet-dry encounters when the main stream is medium (All data are percentages).

Probability of wet-dry encounters		MP								
		C-WSW			C-WSP			C-WSD		
		C-W NW	C-W NP	C-W ND	C-W NW	C-W NP	C-W ND	C-W NW	C-W NP	C-W ND
W-B SW	W-B NW	4.20 %	1.40 %	0.00 %	2.00 %	0.40 %	0.00 %	0.40 %	0.00 %	0.00 %
	W-B NP	0.80 %	1.10 %	0.60 %	0.40 %	0.35 %	0.00 %	0.00 %	0.00 %	0.00 %
	W-B ND	0.00 %	0.60 %	2.60 %	0.00 %	0.00 %	0.60 %	0.00 %	0.00 %	0.00 %
W-B SP	W-B NW	0.60 %	0.00 %	0.00 %	1.20 %	0.40 %	0.00 %	1.00 %	0.00 %	0.00 %
	W-B NP	0.00 %	0.40 %	0.40 %	0.00 %	**7.85 %**	0.00 %	0.00 %	0.40 %	0.00 %
	W-B ND	0.00 %	0.00 %	2.00 %	0.00 %	0.00 %	1.40 %	0.00 %	0.00 %	0.60 %
W-B SD	W-B NW	0.00 %	0.00 %	0.00 %	0.60 %	0.00 %	0.00 %	4.00 %	0.80 %	0.00 %
	W-B NP	0.00 %	0.00 %	0.00 %	0.00 %	0.40 %	0.00 %	1.00 %	1.60 %	0.60 %
	W-B ND	0.00 %	0.00 %	1.00 %	0.00 %	0.20 %	2.00 %	0.00 %	1.20 %	4.90 %

predefined robustness criteria by explicitly matching scenario responses with robustness metrics.

The method emphasizes the coupling relationship between decision variables and key uncertainties. It uses Monte Carlo sampling to generate uncertainty samples and assess the robustness of multi-objective optimization solutions under different scenarios. RMOMC algorithm can effectively identify robust solutions under multi-source uncertainty conditions. Its algorithmic structure consists of six core modules, and the specific flow is shown in Fig. 1.

2.2. Robustness indicators

The *RC*1, *RC*2, *RC*3, and *RC*4 are selected as the robustness metrics, corresponding respectively to the objective function expectation, maximum and minimum cases, objective function standard deviation, and probability thresholds (Zhang et al., 2024). The metrics are computed using the following formulas.

$$RC1(s) = \int f(s,u)p(u)du \tag{1}$$

p(u) represents the probability density function of the random variable *u*, *u* is the neighborhood of the solution *s*. *f(s,u)* represents the objective function. *RC*1: This metric reflects the expected performance across all uncertainties, favoring solutions that perform well on average.

$$RC2(s) = \sup f(s,u) \tag{2}$$

*RC*2: This metric captures worst-case performance, promoting solutions that minimize the maximum possible loss or cost.

$$RC3(s) = \sqrt{\int (f(s,u) - f(s))^2 p(u)du} \tag{3}$$

*RC*3: This metric penalizes variability, encouraging solutions with stable performance across uncertain scenarios.

$$RC4(s) = \Pr(f(s,u) > q|s) \tag{4}$$

Table 3
Scenario probabilities of wet-dry encounters when the main stream is dry (All data are percentages).

Probability of wet-dry encounters		MD								
		C-WSW			C-WSP			C-WSD		
		C-W NW	C-W NP	C-W ND	C-W NW	C-W NP	C-W ND	C-W NW	C-W NP	C-W ND
W-B SW	W-B NW	1.70 %	0.33 %	0.00 %	0.48 %	0.00 %	0.00 %	0.13 %	0.00 %	0.00 %
	W-B NP	0.40 %	0.53 %	0.20 %	0.13 %	0.13 %	0.00 %	0.00 %	0.00 %	0.00 %
	W-B ND	0.00 %	0.28 %	1.20 %	0.00 %	0.08 %	0.20 %	0.00 %	0.00 %	0.00 %
W-B SP	W-B NW	0.53 %	0.20 %	0.00 %	0.68 %	0.13 %	0.00 %	0.33 %	0.00 %	0.00 %
	W-B NP	0.20 %	0.40 %	0.20 %	0.20 %	1.28 %	0.13 %	0.00 %	0.13 %	0.00 %
	W-B ND	0.00 %	0.20 %	1.08 %	0.00 %	0.20 %	0.68 %	0.00 %	0.08 %	0.28 %
W-B SD	W-B NW	0.20 %	0.00 %	0.00 %	0.53 %	0.13 %	0.00 %	2.00 %	0.33 %	0.00 %
	W-B NP	0.00 %	0.20 %	0.00 %	0.28 %	0.33 %	0.13 %	0.73 %	0.88 %	0.28 %
	W-B ND	0.00 %	0.13 %	0.60 %	0.00 %	0.28 %	1.13 %	0.20 %	0.80 %	**3.28 %**

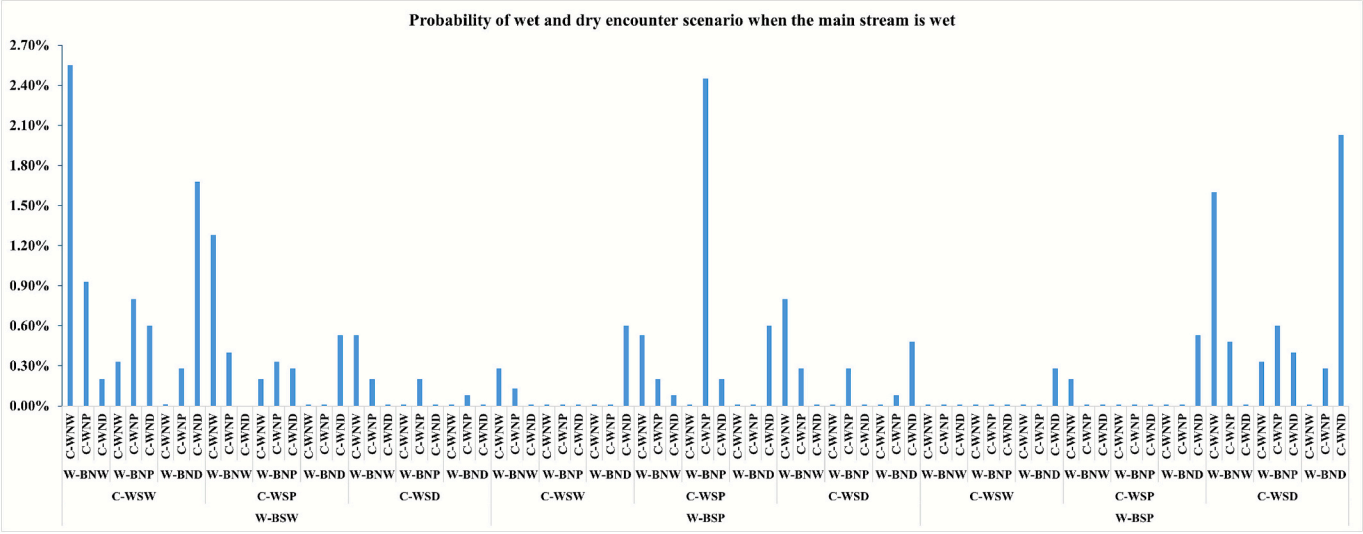

Fig. 3. Scenario probabilities of wet-dry encounters when the main stream is wet.

RC4: This metric represents the probability of exceeding a critical threshold q, useful for risk-sensitive decision-making.

The four-robustness metrics respectively represent central tendency, tail severity, overall dispersion, and tail frequency. Together, these metrics reduce the expected value and dampen variability while also limiting the probability of extremes and bounding the worst consequences, thereby achieving a balanced assessment of both efficiency and safety.

The *NRCi* is defined as the comprehensive performance of a tri-objective function under the specific robustness metrics. The normalized distance from the point to the ideal point is used as its characterization quantity.

$$NRCi_{f1} = NormRCi_{f1} \tag{5}$$

$$NRCi_{f2} = NormRCi_{f2} \tag{6}$$

$$NRCi_{f3} = NormRCi_{f3} \tag{7}$$

$$NRCi = \sqrt{SRCi_{f1}{}^2 + SRCi_{f2}{}^2 + SRCi_{f3}{}^2} \tag{8}$$

To evaluate composite robustness, an index is defined as the weighted sum of the four standardized metrics. All indicators are considered to be equally important, so the arithmetic mean of the four standardized metrics is used to evaluate composite robustness.

$$SRI = \frac{1}{4}\sum_{i=1}^{4} NRCi \tag{9}$$

2.3. Spatial equilibrium-based model for optimal allocation of water resources

Conventional water resources allocation model adopts an efficiency-oriented framework designed by minimizing water deficits, maximizing aggregate economic benefit, and minimizing pollutant emissions (Tian et al., 2019; Zhang et al., 2023; Abdulbaki et al., 2017; Li et al., 2009). While this utilitarian orientation can improve aggregate performance, it is insensitive to allocation equity, tending to concentrate resources in

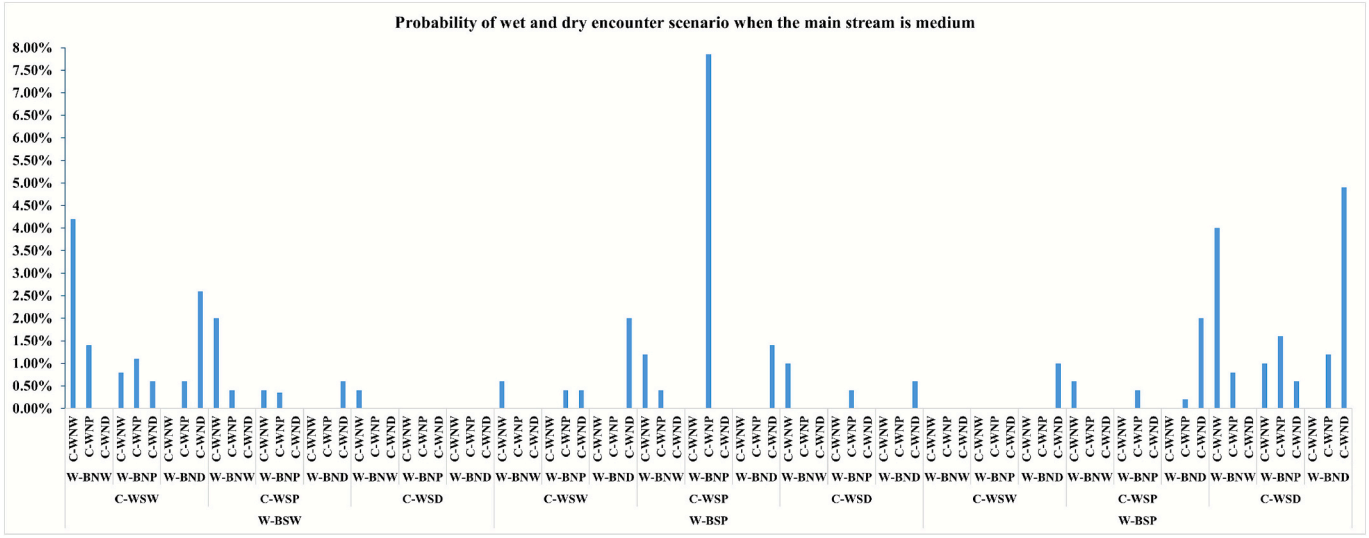

Fig. 4. Scenario probabilities of wet-dry encounters when the main stream is medium.

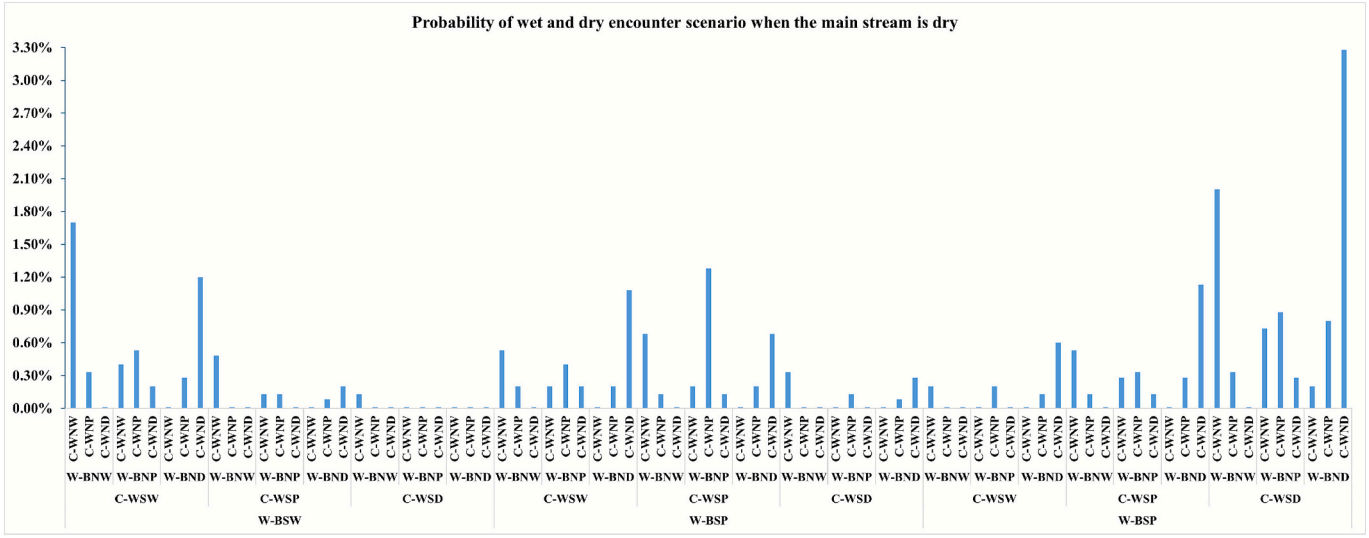

Fig. 5. Scenario probabilities of wet-dry encounters when the main stream is dry.

high benefit regions and to overlook need-based allocation, thereby exacerbating interregional imbalance. For example, areas with large populations but relatively low economic output may struggle to obtain water resources commensurate with their needs.

To address these limitations, the spatial equilibrium-based water resources optimal allocation model focuses on the quantitative and qualitative coupled spatial equilibrium of water resources to achieve the Pareto optimum of balanced, coordinated, equitable, and sustainable development.

(1) Spatial Equalization Objective

In a setting where economically advanced regions, grain-producing bases, and densely populated areas coexist, a singular focus on aggregate economic benefit neither secures distributive fairness nor prevents the under-allocation of water to areas critical for food security and livelihoods. To address this deficiency, spatial equity is incorporated as an explicit optimization objective and quantified using the Gini coefficient-a standard, scale-free measure of interregional inequality. Specifically, compare each region's share of allocated water with its shares of GDP, grain output (or agricultural water demand), and population to quantify deviations, and constructs a composite Gini index as the objective value.

$$PGC = 1 - \sum_{i=1}^{I} (CPQ_i + CPQ_{i-1}) \bullet (CPP_i + CPP_{i-1}) \tag{10}$$

$$AGC = 1 - \sum_{i=1}^{I} (CPQ_i + CPQ_{i-1}) \bullet (CPA_i + CPA_{i-1}) \tag{11}$$

$$GGC = 1 - \sum_{i=1}^{I} (CPQ_i + CPQ_{i-1}) \bullet (CPG_i + CPG_{i-1}) \tag{12}$$

$$minf_2(Q) = \omega_1 \bullet PGC + \omega_2 \bullet AGC + \omega_3 \bullet GGC \tag{13}$$

where PGC represents the Gini coefficient between population and water allocation, AGC represents the Gini coefficient between agricultural water demand and water allocation, GGC represents the Gini coefficient between GDP and water allocation. CPQ_i represents the cumulative share of water supply in space i, CPP_i represents the cumulative share of population in space i, CPA_i represents the cumulative share of agricultural water demand in space i, and CPG_i represents the cumulative share of gross domestic product (GDP) in space i. $\omega_i (i = 1, 2, 3)$ represents the weighting coefficients of the Gini coefficients for population, agricultural water demand, and GDP, and we consider the three Gini coefficients to be equally important, so $\omega_1 = \omega_2 = \omega_3 = 1/3$.

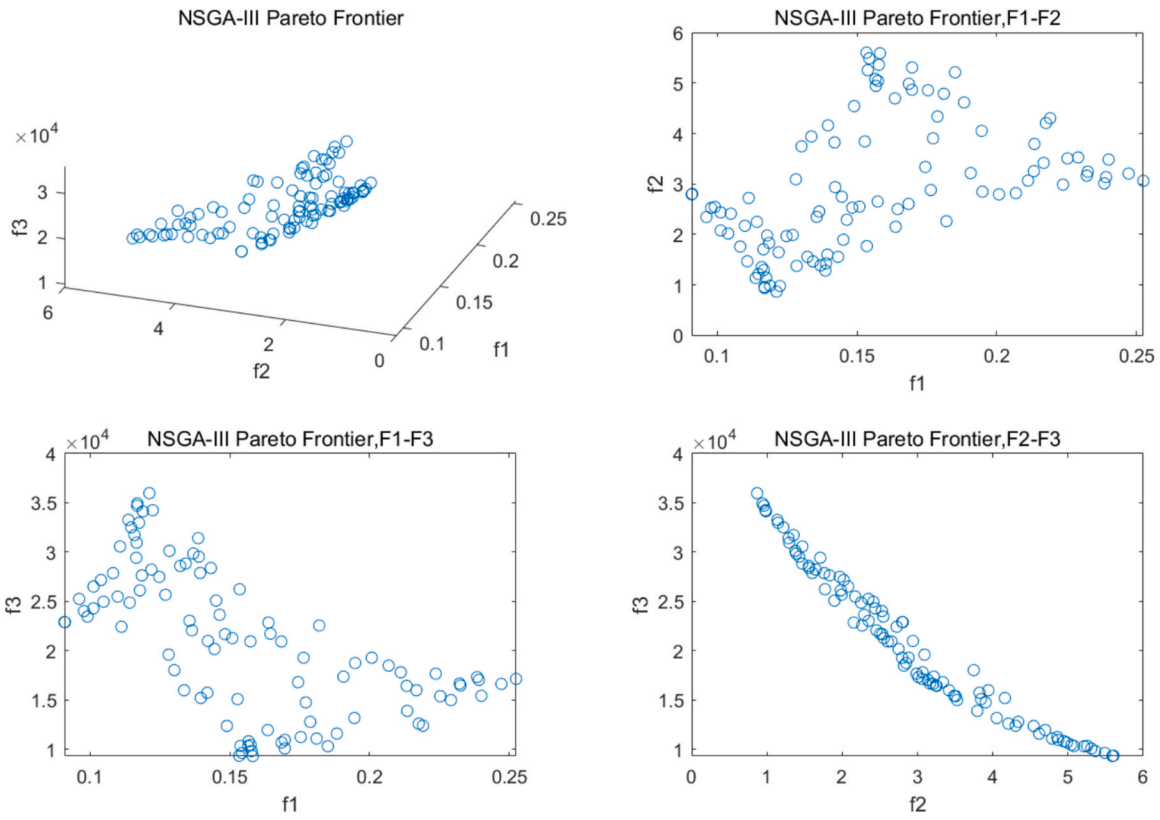

Fig. 6. Classical Robust Optimization Pareto Frontier. The f1 represents the value of Spatial Equalization Objective-Gini Coefficient; the f2 represents the value of Social Objective-Water Deficit, the f3 represents the value of Sustainable Development Objective-Pollutant Emission(ton).

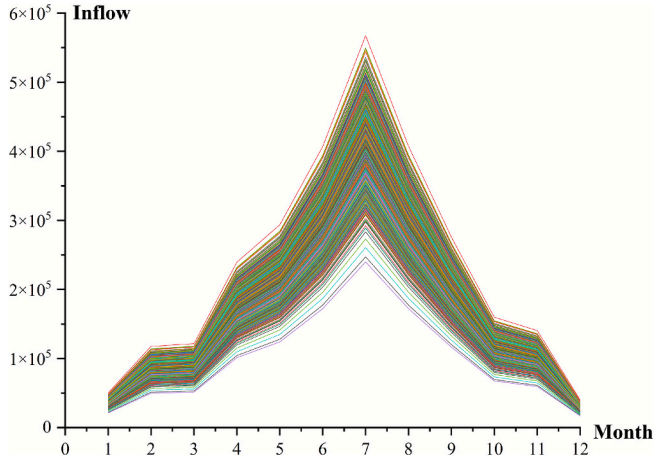

Fig. 7. Sample annual inflow volume (10^4 m^3). The horizontal axis represents months, and the vertical axis represents monthly inflow.

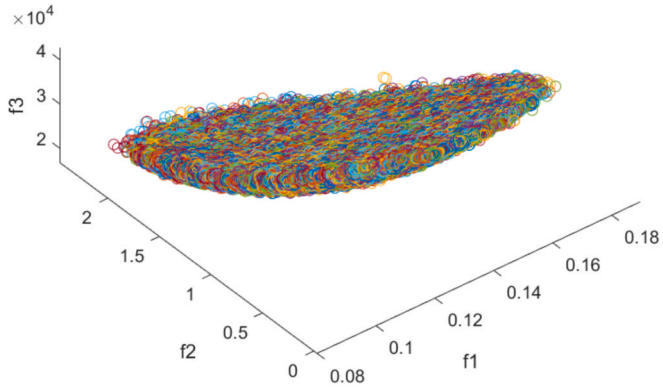

Fig. 8. 1200 Pareto frontier sets under 1200 inflow scenarios. The f1 represents the value of Spatial Equalization Objective-Gini Coefficient; the f2 represents the value of Social Objective-Water Deficit, the f3 represents the value of Sustainable Development Objective-Pollutant Emission(ton).

(2) Social objective

While following the principle of spatial equilibrium, the allocation needs to try to meet the water demand of each sector by targeting the sum of the water deficit rates of each sector in the study area:

$$minf_1(Q) = \sum_{j=1}^{J}\sum_{k=1}^{K}\alpha_k\left(\frac{\sum_{t=1}^{T}D_{jkt} - \sum_{t=1}^{T}\sum_{i=1}^{I}Q_{ijkt}}{D_{jk}}\right)^2 \quad (14)$$

$$Q_{ijkt} = P_{ijkt} * r * AW \quad (15)$$

where r is the uncertainty variable, r $N(1, 0.07^2)$; D_{jkt} denotes the water demand of water sector k in city j at time t; Q_{ijkt} denotes the amount of water supplied by water source i to water sector k in city j at time t. α_1, α_2, α_3 are the water allocation weights for domestic water use, primary industry water use and secondary and tertiary industry water resources,

Table 4
Optimal solution numbering for different robustness metrics.

No.	*RC*1	*RC*2	*RC*3	*RC*4	*SRI*
Gini	407	897	831		551
WD	613	613	379	379	613
P	662	662	662	662	622
SRC	1068	1068	116	1081	587

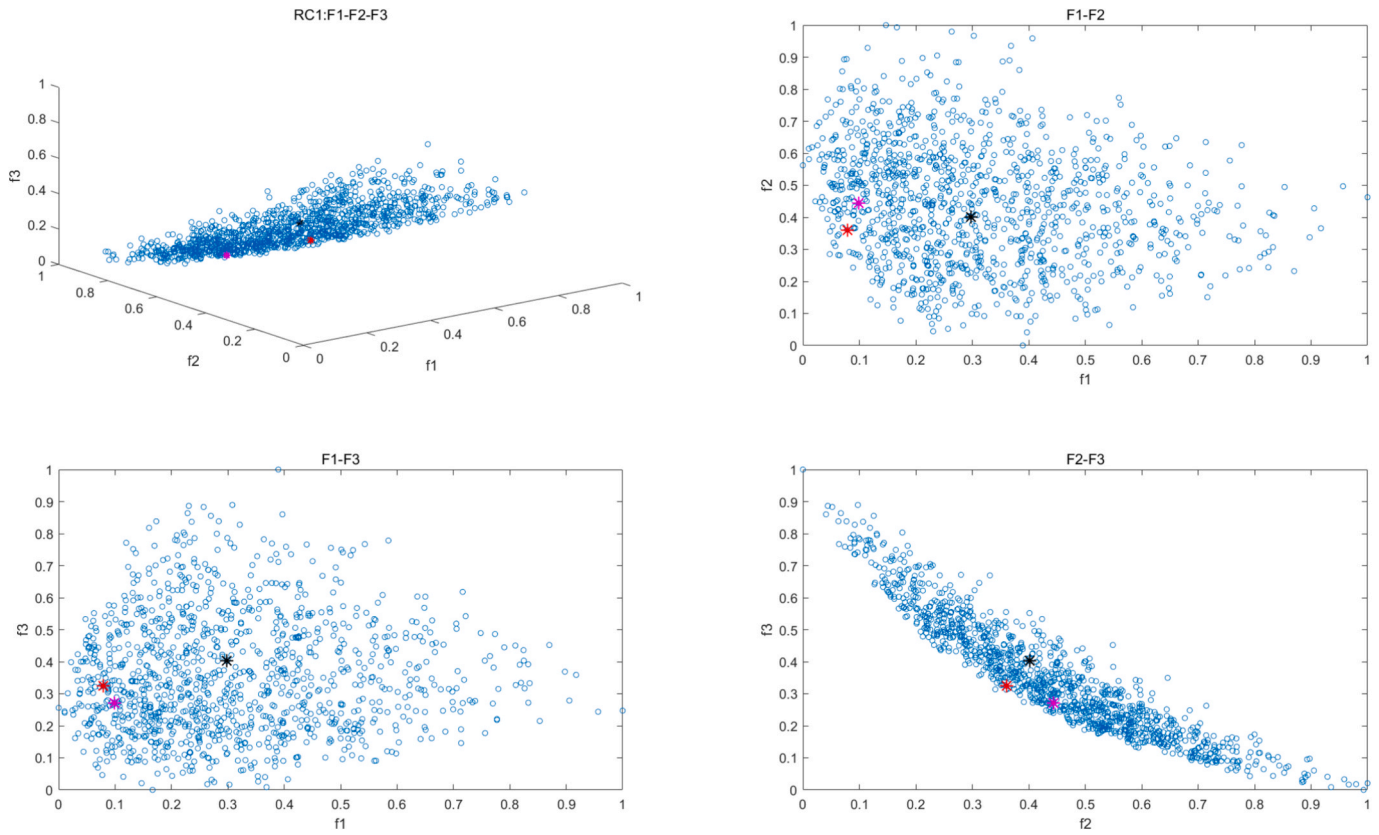

Fig. 9. Robustness performance of 1201 solutions (1200 robust model solutions, 1 deterministic model solution) in RC1 (blue circle: all solutions; red "*": integrated robustness optimal solution; pink "*": integrated robustness optimal solution of RC1; black "*": classical robust optimization solution); The f1 represents the performance of the robustness for Gini Coefficient the f2 represents the robustness performance for Water Deficit, the f3 represents the robustness performance for Pollutant Emission. (For interpretation of the references to colour in this figure legend, the reader is referred to the web version of this article.)

with values of 0.5, 0.2 and 0.3 respectively; AW denotes the total surface water resources in the study area; P_{ijkt} is the decision variable of the model, which represents the percentage of the total surface water resources AW supplied by water source i to water sector k of computational unit j in time period t.

(3) Sustainable Development Objective

While following the principles of equilibrium and equity, and in conjunction with the problem of severe water pollution in the study area, the configuration still needs to take into account typical pollutant discharges, intending to minimize typical pollutant discharges in the study area as a whole:

$$minf_3(Q) = \sum_{j=1}^{J}\sum_{k=1}^{K} d_{jk} pol_{jk} \sum_{i=1}^{I}\sum_{t=1}^{T} Q_{ijkt} \tag{16}$$

Where d_{jk} denotes the typical pollutant discharge per unit volume of water in water sector k in calculation unit j (ton/m^3); and pol_{jk} denotes the typical pollutant discharge coefficient of water sector k in calculation unit j.

(4) System Equilibrium Constraints

Harmonization refers to the state of coherence and consistency between systems and is often used to describe constructive and synergistic interactions. Current research on spatial equilibrium focuses on the spatial equilibrium of water resources and ignores the spatial equilibrium of the ecological environment. To evaluate the coordinated relationship between the water resources system, socio-economic system, and environmental environment system, the degree of coupled coordination is used as a criterion for the spatial equilibrium of the ecological environment. The three subsystems are characterized by three representative indicators: per capita water resources, per capita GDP, and pollutant emissions per 10,000 CNY of GDP. The specific calculation formulas are presented as follows:

$$C_{1,j} = \frac{\sum_{k=1}^{K}\sum_{i=1}^{I} Q_{ijk}}{Pop_j} \tag{17}$$

$$C_{2,j} = \frac{gdp_j \bullet \sum_{k=1}^{K}\sum_{i=1}^{I} Q_{ijk}}{Pop_j} \tag{18}$$

$$C_{3,j} = \frac{\sum_{k=1}^{k} d_{jk} pol_{jk} \sum_{i=1}^{I} Q_{ijk}}{gdp_j \bullet \sum_{k=1}^{K}\sum_{i=1}^{I} Q_{ijk}} \tag{19}$$

where, Pop_j denotes the population of calculation unit j; gdp_j denotes the gross domestic product of calculation unit j; d_{jk} denotes the typical pollutant discharge per unit volume of water in water sector k in calculation unit j (ton/m^3); and pol_{jk} denotes the typical pollutant discharge coefficient of water sector k in calculation unit j.

The coupled coordination of the composite system is:

$$C_j = \frac{3\sqrt{c_{1,j} \bullet c_{2,j} \bullet c_{3,j}}}{c_{1,j} + c_{2,j} + c_{3,j}} \tag{20}$$

$$T_j = \alpha C_{1,j} + \beta C_{2,j} + \gamma C_{3,j} \tag{21}$$

$$D_j = \sqrt{C_j \bullet T_j} \tag{22}$$

D_j is the degree of coupled coordinated development, and α, β, γ are the weights of each system, all of which are 1/3. $D_j \geq 0.7$ is taken as one of the constraints to realize the spatial equilibrium of the ecological environment.

In addition to the above constraints, they also include hydraulic

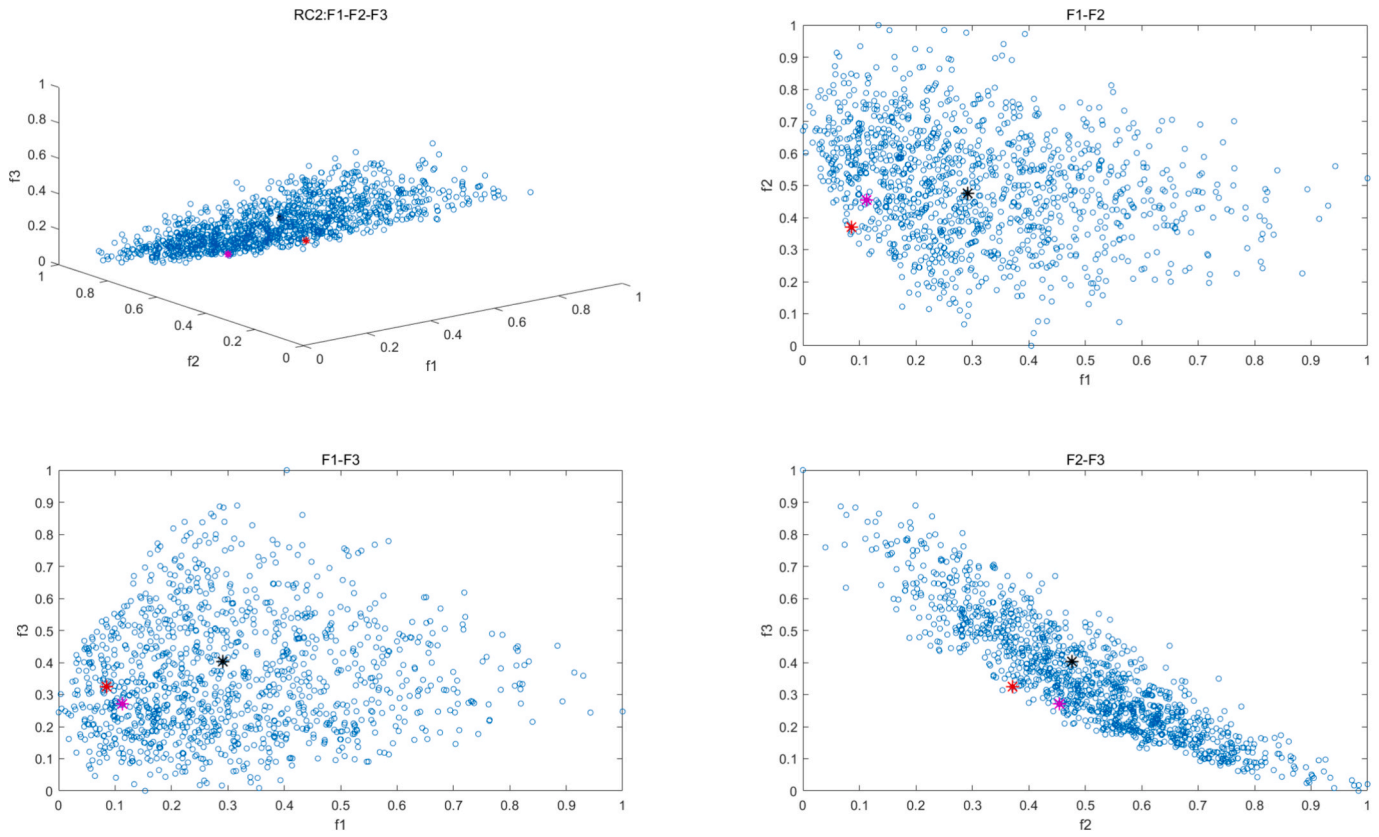

Fig. 10. Robustness performance of 1201 solutions (1200 robust model solutions, 1 deterministic model solution) in RC2 (blue circle: all solutions; red "*": integrated robustness optimal solution; pink "*": integrated robustness optimal solution of RC2; black "*": classical robust optimization solution); The f1 represents the performance of the robustness for Gini Coefficient, the f2 represents the robustness performance for Water Deficit, the f3 represents the robustness performance for Pollutant Emission. (For interpretation of the references to colour in this figure legend, the reader is referred to the web version of this article.)

linkage constraints, water balance constraints, and non-negative variables constraints (Jia et al., 2006).

3. Study area

The Huaihe River Basin is located in the central-eastern part of China, spanning 111°55′-121°25′ E longitude and 30°55′-36°36′ N, with a total watershed area of approximately 190,000 km^2 (see Fig. 2a). Among them, the Upper Middle River Region (UMHR, defined as the area above the Bengbu lock) covers a total of 15 municipalities in Henan and Anhui provinces. When constructing the schematic concept map of the study area's water resources allocation system, the computational units were delineated by overlaying hydrological and administrative boundaries, further refined based on existing water supply, conveyance, and drainage networks. This abstraction facilitates the characterization of each unit's socioeconomic attributes and patterns of water resources development and use, while simplifying the problem structure, clarifying supply–demand coupling, and enabling rigorous model formulation and analysis. The generalized structure of the UMHR water resources system is shown in Fig. 2 b.

Digital elevation model (DEM) data were obtained from the open access SRTM dataset. Hydrological data, including station locations and monthly runoff for approximately 60 years (1956–2010), were sourced from the China Hydrological Yearbook. Socioeconomic data were extracted from the China Statistical Yearbook, the Henan Statistical Yearbook, and the Anhui Statistical Yearbook. Information on water supply routes, drainage networks, and water use units was provided by the Huaihe River Commission of the Ministry of Water Resources.

4. Results and discussion

4.1. Analysis of the probability of the incoming water wet and dry encounters in the main stream – interval

Based on the R-Vine Copula model (Copca Maya and Fuentes Mariles, 2025), the abundance encounter probabilities of the main stream and the interval inflows in the basin were calculated, and the results are shown in Tables 1,2,3 and Figs. 3,4,5. There are five nodes involved in the variables, in which: M denotes the main stream, C-W denotes the interval from the Changtaiguan to Wangjiaba, W-B denotes the interval from Wangjiaba to Bengbu lock, and S and N represent the south bank and north bank of each interval, respectively. The incoming water scenarios are categorized into three states: wet (W), medium (P) and dry (D). For example, C-WSD represents the "inflow scenario of the south bank of the interval from Changtaiguan to Wangjiaba during the dry period".

For the Huaihe River Basin, the probability that the main-stream and interval inflows fall within the same wet year, same normal year, and same dry year is 2.55 %, 7.85 %, and 3.28 %, respectively. The probability that the main stream and interval inflows exhibit fully synchronized wet–normal–dry conditions is 13.68 %, whereas the probability of asynchronous wet–dry encounters reaches 86.32 %. Notably, the likelihood of wet–dry asynchrony is 6.3 times greater than the probability of wet–dry synchrony. Among the three hydrological states, synchronization in normal years occurs most frequently, with its probability being 3.07 times that of synchronized wet years and 2.39 times that of synchronized dry years.

Under the condition that the main stream is in a dry year, the probabilities that the four interval inflows simultaneously fall into wet,

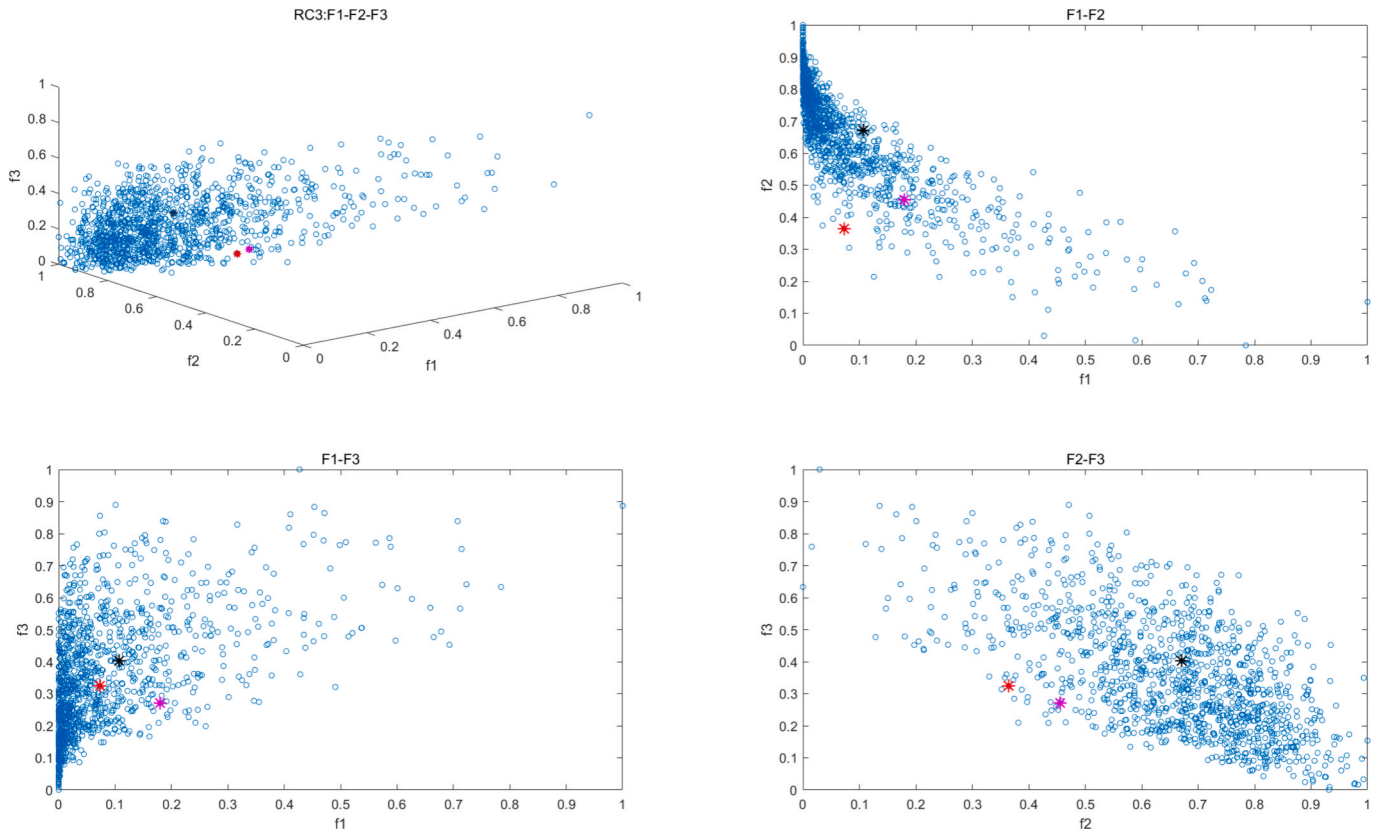

Fig. 11. Robustness performance of 1201 solutions (1200 robust model solutions, 1 deterministic model solution) in RC3 (blue circle: all solutions; red "*": integrated robustness optimal solution; pink "*": integrated robustness optimal solution of RC3; black "*": classical robust optimization solution); The f1 represents the performance of the robustness for Gini Coefficient, the f2 represents the robustness performance for Water Deficit, the f3 represents the robustness performance for Pollutant Emission. (For interpretation of the references to colour in this figure legend, the reader is referred to the web version of this article.)

normal, and dry states are 28.1 %, 33.9 %, and 25.0 %, respectively. Among these, synchronization in the normal-year state occurs most frequently. There are 81 scenarios under the conditions of wet, medium and dry conditions, and the probability of the four inter-area inflows with the same wet, the same medium, and the same dryness is the largest under each condition, which indicates that the encounter of the wetness and dryness of the inter-area inflows in the Huaihe River Basin in the area above the Bengbu lock is relatively consistent with that of the wetness and dryness of the dry river. Accordingly, the scenario in which all five regions of the study area experience a normal water year is selected as the representative case scenario for further analysis.

4.2. Optimal allocation of water resources based on classical robust optimization algorithm

In this section, based on the classical robust optimization method proposed by Deb (Deb et al., 2002), the neighborhood parameter δ is set to be 0.2. The number of stratification H to be 50. A robustly superior water allocation scheme is obtained, whose three-dimensional Pareto front is shown in Fig. 6. The results show that the composite Gini coefficient of the optimized study area is distributed between 0.09 and 0.17, the sum of sectoral water scarcity rates ranges from 0.4 to 2.0. The pollutant emissions are between 18,000 and 38,000 tons. This Pareto frontier provides decision-makers with various trade-off options that facilitate the selection of specific implementation options based on different preferences.

For example, if the prioritized water deficit rate is ranked 1 or 2, the composite Gini coefficients for the corresponding allocation scenarios are 0.102 and 0.121, respectively, which the decision maker can judge. However, a single Pareto frontier cannot quantify the robustness of each allocation scheme under uncertain inflow conditions, nor can it reveal how inflow uncertainty propagates through the system.

Therefore, the solution closest to the ideal point in the Pareto frontier is selected as the classical robust solution and analyzed compared with the comprehensive robust solution obtained from the RMOMC algorithm search to assess its stability and adaptability under multi-source uncertainty conditions.

4.3. Optimal allocation of water resources based on the RMOMC algorithm

The primary runoff in the area above Changtaiguan, the interval inflow on the north and south bank of the Changwang interval, and the north and south bank of the Wangbeng area all fall within medium water years as the study case scenario. The natural annual runoff in the watershed is used as the uncertainty variable, Monte Carlo sampling is applied, and the resulting sample distribution is shown in Fig. 7. In the second part of the step of applying RMOMC, a set of 1200 Pareto fronts is generated (Fig. 8). In the fourth part of the step, the closest solution to the ideal point in each Pareto frontier was generated based on the distance of each solution to the ideal point, yielding a total of 1,200 candidate robust solutions.

4.4. Assessing the robustness of the solution

To evaluate the performance of each solution in the solution set S on the four robustness metrics, the three objective-function values must first be computed for every inflow scenario and then evaluate the performance of the three objective functions on the four robustness metrics. For 1200 incoming samples, each solution needs to compute the

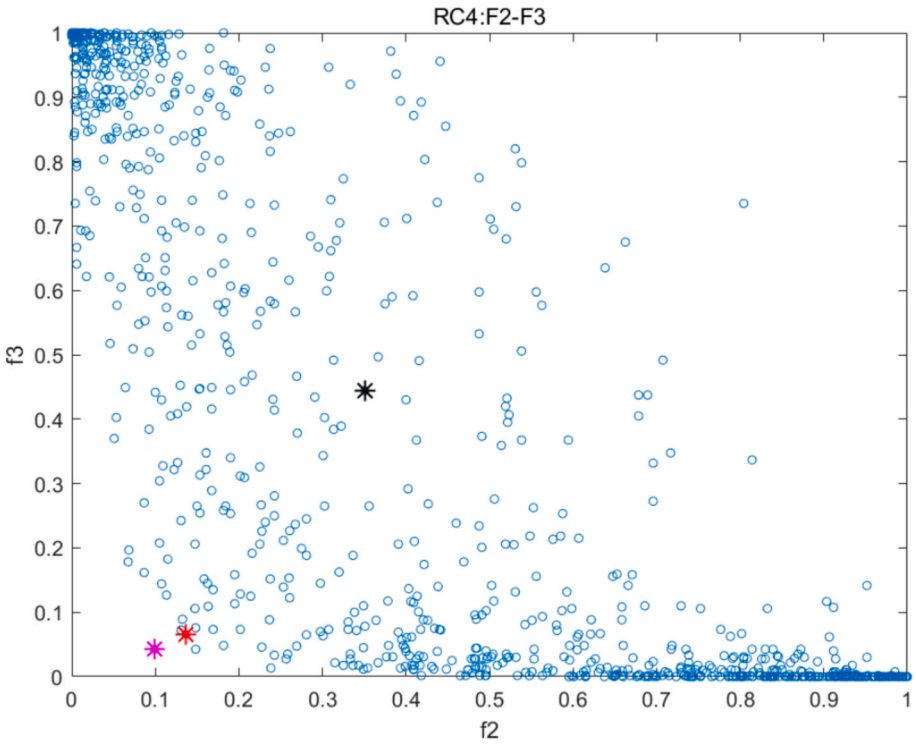

Fig. 12. Robustness performance of 1201 solutions (1200 robust model solutions, 1 deterministic model solution) in RC4 (blue circle: all solutions; red "*": integrated robustness optimal solution; pink "*": integrated robustness optimal solution of RC4; black "*": classical robust optimization solution); The f2 represents the robustness performance for Water Deficit, the f3 represents the robustness performance for Pollutant Emission. (For interpretation of the references to colour in this figure legend, the reader is referred to the web version of this article.)

Table 5
Robustness configuration scheme of spatial equilibrium model for r = 1.

Region	Water supply ($\times 10^6 m^3$)	Water demand($\times 10^6 m^3$)	Water deficit
R1	43.07	59.56	27.68 %
R2	56.88	62.18	8.52 %
R3	286.28	336.71	14.98 %
R4	1273.18	1330.66	4.32 %
R5	998.78	1378.06	27.52 %
R6	50.77	61.44	17.36 %
R7	488.47	700.25	30.24 %
R8	873.53	921.62	5.22 %
R9	374.47	567.09	33.97 %
R10	1083.82	1361.95	20.42 %
R11	421.60	627.78	32.84 %
R12	1507.02	1507.02	0.00 %
R13	992.52	1297.40	23.50 %
R14	826.21	1285.68	35.73 %
R15	515.83	629.04	18.00 %
Total	9699.05	12126.44	19.24 %

objective function values 1200 times and then compute *RC1, RC2, RC3, RC4, SRC*, and *SRI*, respectively. Then, the corresponding solution number can be found from the minimum value of each robustness metric. The objective function values are normalized for the integrated robustness performance of the solutions under different metrics. Then, the distance from the normalized point to the ideal point is calculated. The closest point to the ideal point is selected as the optimal integrated robustness solution under the robustness metrics. The optimal solution numbers for the robustness dimension of each objective function are shown in Table 4.

Figs. 9–12 represents the robustness performance of the three objective functions under *RC*1 ~ *RC*4. Because the robustness value of the Gini-coefficient objective function is zero under *RC*4, Fig. 9 only displays the performance of objective function 2 and objective function 3 in terms of robustness on *RC*4. The four figures show the performance of the 1200 RMOMC algorithm solutions (blue hollow circles), the RMOMC algorithm globally integrated robustness optimal solutions (red "*"), and classical robust optimization algorithm solutions (black "*") on the four robustness dimensions, and under each robustness metric, the configuration scheme with the best-integrated robustness under the metric is also labeled (pink "*"). Although there are some dominated solutions in the four plots, it is also possible to form four approximate Pareto fronts, demonstrating a degree of competitiveness of the three objective functions on all four robustness dimensions.

From the first graph in Fig. 9, it can be noticed that the leftmost extreme point is the smallest for *RC*1 of f_1, but the largest for *RC*1 of f_2; similarly, the rightmost extreme point is the smallest for *RC*1 of f_2, but the largest for *RC*1 of f_1. Similarly, this phenomenon also exists in the robustness metrics *RC*2, *RC*3, and *RC*4. More importantly, as shown in Table 4, the solution closest to the ideal point differs in each of the four robustness dimensions. If the basin management wants a robust water allocation solution, the decision maker may need to choose from these four solutions. Specifically, for *RC*1, the No. 407 solution is optimal in terms of robustness to the composite Gini coefficient, the No. 613 solution is optimal in terms of robustness to the rate of water scarcity, and the No. 662 solution is optimal in terms of robustness to the pollutant discharge. For *RC*2 and *RC*3, the schemes with optimal robustness of the composite Gini coefficient are No.897 and No.831, respectively. For *RC*4, the composite Gini coefficient does not exceed 0.2 for any of the 1200 inflow samples, so the value of 0 at *RC*4 is robust for all the configuration schemes in this robustness dimension.

Because there are many non-inferior solutions in the Pareto frontier, the decision maker needs to select from them. The decision maker needs to select from the non-inferior solutions and measure between different robustness metrics or select the solutions by combining the robustness. As shown in the *SRC* rows in Table 4, the solutions closest to the ideal point for *RC*1, *RC*2, *RC*3, and *RC*4 are NO.1068, NO.1068, NO.116, and

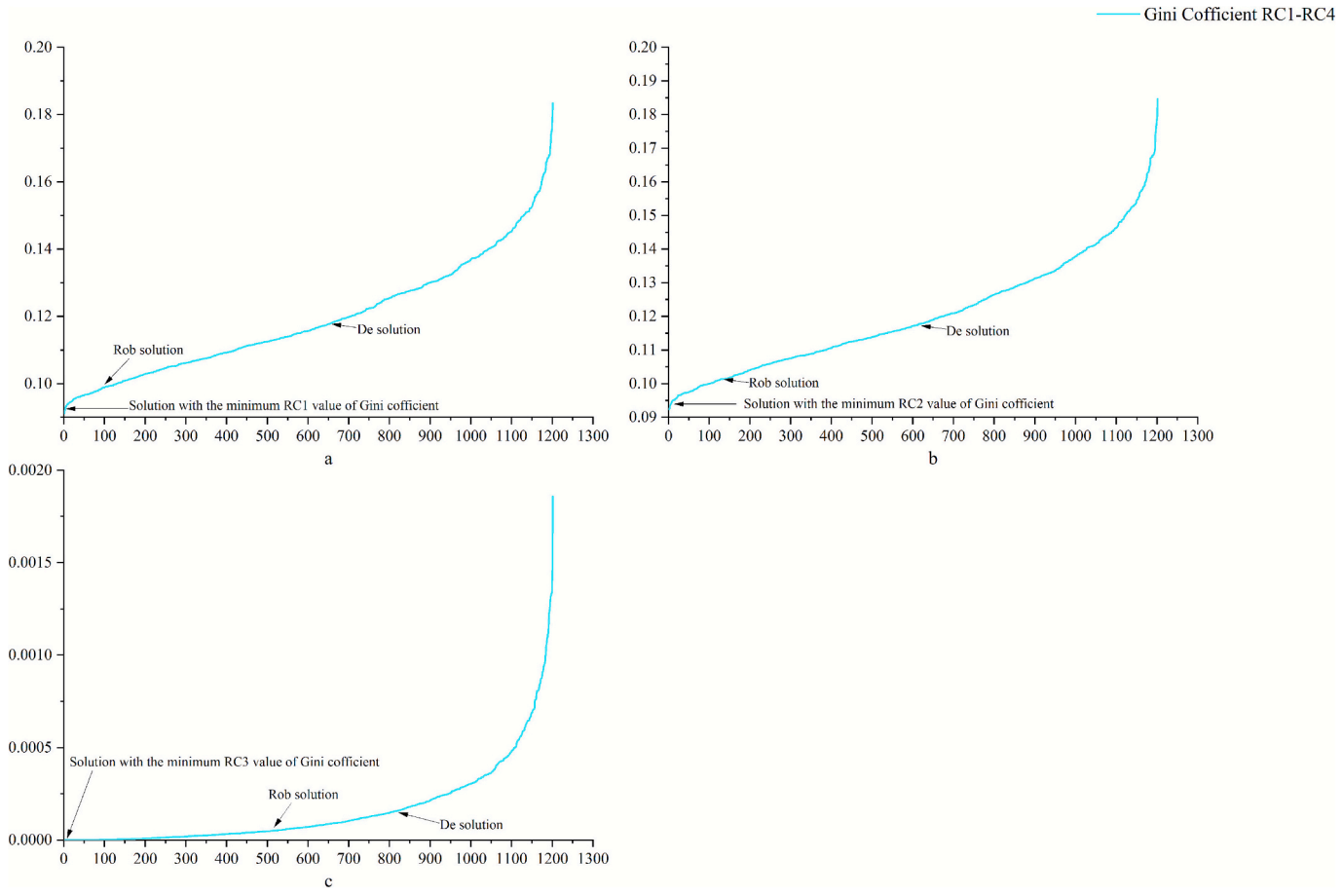

Fig. 13. Robustness performance of 1201 solutions in the composite Gini coefficient (a:RC1, b:RC2, c:RC3).

No.1081, respectively, and the optimal solution in terms of combined robustness is NO.587.

4.5. Results of the water allocation program

The NSGA-III algorithm (Blank et al., 2019) was applied to solve the spatial equilibrium-based optimal water resources allocation model, and the RMOMC algorithm was combined to identify the optimal allocation scheme with integrated robustness as No. 587, which is shown in Table 5 under the average water inflow (i.e., uncertainty variable $r = 1$).

Under deterministic condition ($r = 1$), the overall water deficit rate in the UMHR is 19.24 %. The specific amount of water shortage is 2.43 billion m^3, of which the water deficit in the south bank area of the Huaihe River is 1.48 billion m^3, and that in the north bank area is 0.95 billion m^3. The deficit rate is 45.42 % lower than that in the classical allocation model with an integrated robust solution of 35.23 %, and the difference in specific allocation schemes will be described in the next section.

Based on the allocation results, the sectoral water use shares were analyzed, showing that the domestic sector, agriculture, and the secondary and tertiary industries account for 23.8 %, 44.2 %, and 32 % of total water use, respectively. This allocation strategy demonstrates a relatively balanced water allocation model with no apparent bias toward any sector. In the spatial equilibrium model allocation, although the water supply weights of the domestic, secondary, and tertiary sectors are given higher priority, the spatial equilibrium goal adopted focuses more on achieving the complete satisfaction of the water needs of all sectors. Implementing such a water allocation strategy ensures the prioritization of domestic and industrial water supply. Still, the spatial equilibrium objective seeks to ensure that the water demand of all sectors is fully met, which leads to a potential competitive relationship with the water deficit rate objective in the model design. That is, while the model aims to support socio-economic development through efficient water allocation, it also strives to balance agricultural production's water needs with ecosystems' needs.

In this section, based on the Gini coefficient, the coupling degree of coordination is also used to measure the spatial balance of the ecological environment to characterize the spatial balance of water resources quality. As shown in section 2.3, the spatial equilibrium allocation model of water resources takes the coupling degree of the water resources-socio-economic-ecological environment system as one of the constraints. The results show that the coupling degree of the system in each region is above 0.75, which is in a basic state of coordination. The spatial equilibrium of water resource quality has been realized.

4.6. Comparing RMOMC algorithm robust solutions with classical robust optimization robust solutions

To visually compare the robustness of 1200 robust solutions of the RMOMC algorithm and 1 classical robust optimization algorithm solution over the three objective functions, the robustness of each solution over the three objective functions is shown in Fig. 13, Fig. 14, and Fig. 15, where Rob solution denotes the combined robustness optimal solution of the RMOMC algorithm and De solution denotes the classical robust optimization optimal solution.

As shown in Fig. 13, ranking the robustness of the composite Gini coefficients from smallest to largest, the composite robust solution outperforms the classical robust solution. Specifically, on the $RC1-RC3$ metrics, the robustness of the composite robust solution is better than 92.4 %, 91.1 %, and 57.3 % of the solutions, respectively; however, the

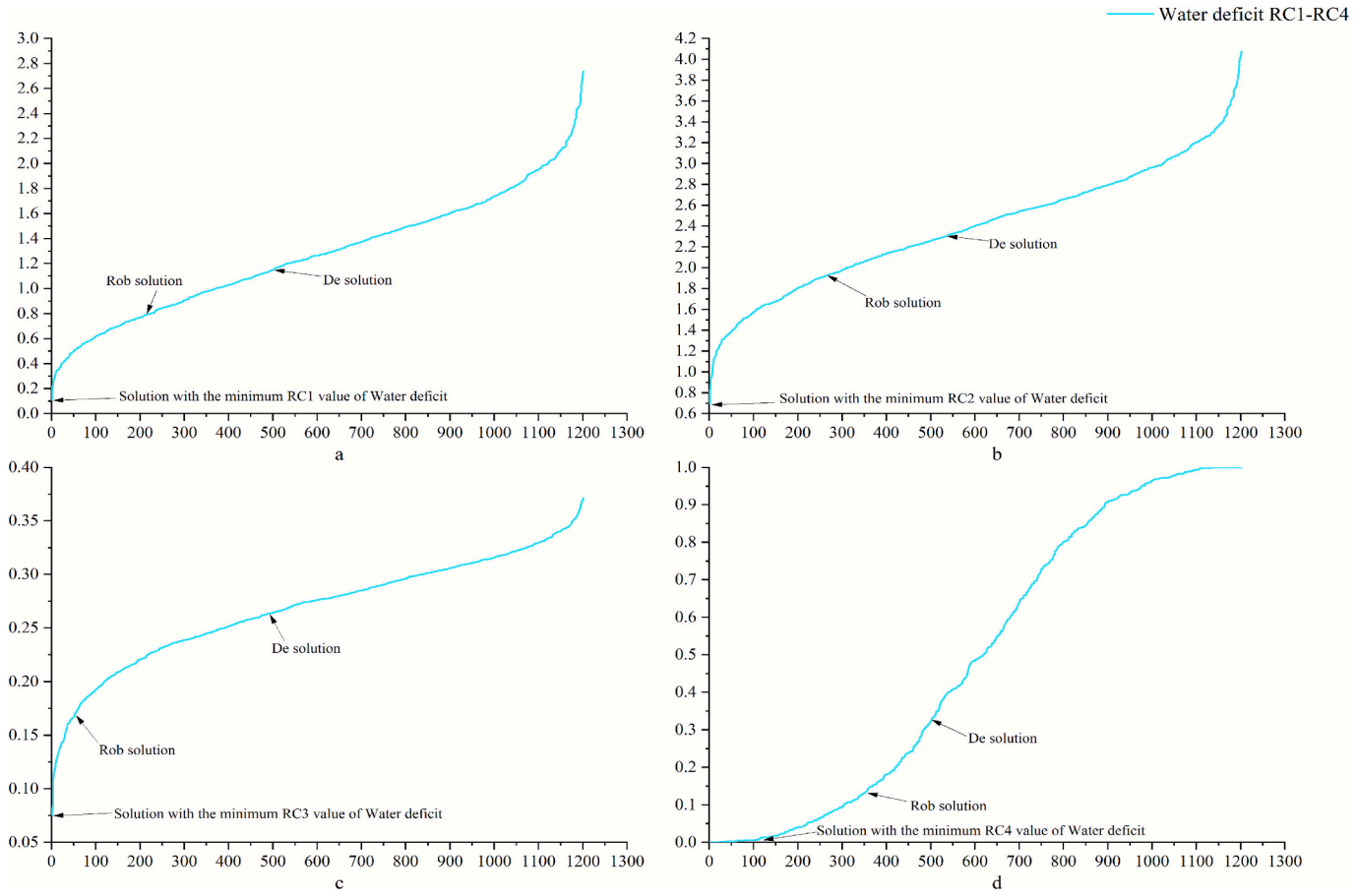

Fig. 14. Robustness performance of 1201 solutions on water deficit rates (a:RC1, b:RC2, c:RC3, d:RC4).

robustness of the classical robust solution is better than only 44.1 %, 45.5 %, and 33.2 % of the solutions. To analyze the specific performance of the integrated robust solution and the classical robust solution, the ratio of $RC(De)/RC(Rob)$ is used in this section to reflect the comparison of the robustness of the two solutions. The $RC(De)/RC(Rob)$ is 1.205, 1.189, and 1.471 in the four robustness dimensions, respectively, which implies that, for the rate of water deficits, the classical robust solution in the four robustness dimensions may result in 20.5 %, 18.9 % and 47.1 % more variability, highlighting the advantage of the integrated robust solution in ensuring spatial equilibrium robustness. The threshold in this case for the Gini coefficient objective was set at 0.2. None of the Gini coefficients across the 1,200 configuration samples exceeded this threshold, indicating that all configuration scenarios achieved spatial equilibrium under all inflow conditions.

Arranging the robustness of water deficit rates from smallest to largest, as shown in Fig. 14, the robustness of the integrated robust solution is also superior to that of the classical robust solution, but the difference in robustness between the two is smaller relative to the integrated Gini coefficient. Specifically, the robustness of the composite robust solution outperforms 81.1 %, 76.4 %, 93.5 %, and 70.3 % of the other solutions in the four robustness dimensions, respectively. In contrast, the robustness of the classical robust solution only outperforms 57.1 %, 55.3 %, 51.8 %, and 56.8 % of the solutions. The $RC(De)/RC(Rob)$ is 1.101, 1.182, 1.493, and 2.567 in the four robustness dimensions, respectively, which implies that, for the rate of water scarcity, the classical robust solution in the four robustness dimensions may lead to 10.1 %, 18.2 %, 49.3 %, and 156.7 % more variability, further emphasizing the advantage of the integrated robust solution in ensuring the robustness of the water deficit rate.

Ranking the robustness of pollutant emissions from smallest to largest, as shown in Fig. 15, the robustness of the integrated robustness solution is significantly better than the classical robustness solution. Specifically, the integrated robustness solution outperforms approximately 59.3 % of the solutions in the four robustness dimensions, while the classical robustness solution only outperforms approximately 36.5 %. Similarly, the robustness difference between the two solutions by $RC(Rob)/RC(De)$ is further quantified, and it can be found that for $RC1$ to $RC3$, the value of $RC(Rob)/RC(De)$ is about 1.077, and for $RC4$ the ratio is 6.74. This demonstrates that, for the cost of contamination, the integrated robust solution in $RC1$ to $RC3$ is about 7 % more robust than the classical robust solutions by 7.7 % and 574 % in $RC4$, and this significant difference emphasizes the importance of integrated robust solutions in mitigating potential risks.

To analyze the combined performance of each solution on the four robustness dimensions, this section reflects the combined robustness of all solutions under a single robustness metric, Pareto Frontier, by the distance from the non-inferior solution to the origin in that metric. As shown in Fig. 16, the combined performance of the synthesized robust solutions is significantly better than the classical robust solutions in $RC1$ to $RC4$. Specifically, the combined robustness performance of the integrated robust solution in $RC1$ and $RC4$ is better than 92.7 % and 88.8 % of the solutions, respectively. The combined performance in $RC2$ and $RC3$ is better than basically all the solutions (better than 98.8 % and 99.6 % of the solutions). However, the classical robust solution performs slightly worse in terms of robustness in all the four robustness dimensions, and is better than 86.8 %, 90.9 %, 50.7 %, and 79.5 % of the solutions. Based on the ratio of $Dis(Rob)/Dis(De)$, it can be found that the combined robustness of the integrated robust solution is 8.2 %, 9.6 %, 60.1 %, and 26.1 % better than the classical robust solution in the four robustness dimensions, which shows the combined performance

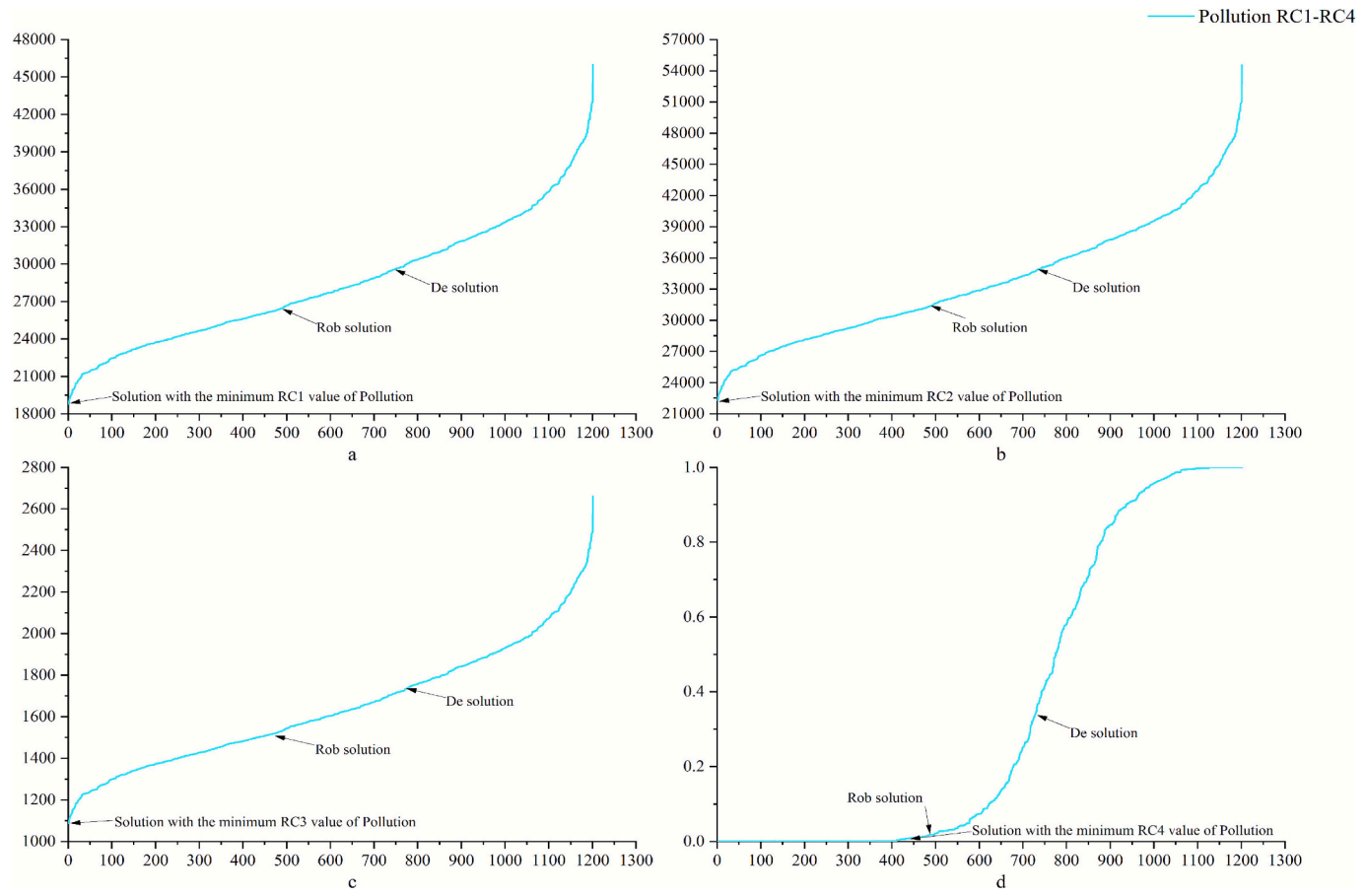

Fig. 15. Robustness performance of 1201 solutions on pollutant emissions (a:RC1, b:RC2, c:RC3, d:RC4).

superiority of the integrated robust solution in each robustness metric.

Similarly, the combined robustness of the integrated and classical robust solutions was compared across three objectives and overall performance. Fig. 17 shows that the integrated robust solution performs more robustly in the Gini coefficient, water scarcity rate, and pollutant emissions. Specifically, for the integrated Gini coefficient, the robustness of the integrated robust solution is better than 67.7 % of the solutions, while the robustness of the classical robust solution is better than 20.2 % of the solutions; for the water scarcity rate, the robustness of the integrated robust solution is better than 80.1 % of the solutions, while the robustness of the classical robust solution is better than 55.3 % of the solutions. For the pollutant emissions, the robustness of the integrated robust solution is better than 51.1 % of the solutions. In comparison, the robustness of the classical robust solution is better than 51.1 % of the solutions. Solutions, while the robustness of the classical robust solution is only better than 36.5 % of the solutions. Based on the ratio of $SRI(Rob)/SRI(De)$, the classical robust solution is 40.2 % more uncertain than the integrated robust solution in terms of the integrated Gini coefficient, 54.5 % more uncertain than the integrated robust solution in terms of water scarcity, and 36.6 % more uncertain than the integrated robust solution in terms of pollutant emissions. In terms of global composite robustness, the ratio of $Dis(Rob)/Dis(De)$ is 0.688, which means that the composite robustness of the integrated robust solution is 45.3 % higher than that of the classical robust solution.

4.7. Analysis of specific scenarios for water allocation based on spatial equilibrium

This section compares the configuration scheme of the integrated robust solution of the spatial equilibrium model and the configuration scheme of the classical robust solution of the spatial equilibrium model; as shown in Fig. 18, the two configurations supply close to the same amount of water, and the configuration scheme of the integrated robust solution mainly improves the supply of water to the cities with larger water demand, such as R12, R10, and R4.

Specifically for the water supply sector, the differences between the two allocation scenarios are mainly between the water supply for the primary sector and the water supply for the secondary and tertiary sectors since the water supply for residential use needs to be secured. Fig. 18(b) reveals the change in the share of water supply in the agricultural sector, where positive values reflect an increase in the share of water supply in the primary sector for the integrated robust solution relative to the classical robust solution, while negative values indicate a relative decrease. Fig. 18(b) shows that 13 out of the 15 water use units show a decrease in agricultural water supply, with particularly significant performance in R12, R5, and R8. The reason for this change is that, on the one hand, reducing water supply to agriculture and increasing water supply to secondary and tertiary sectors can improve spatial balance and effectively reduce pollutant discharge, thus enhancing robustness in both objectives; on the other hand, given the highest allocation weight of water for domestic use and the high efficiency of water use in secondary and tertiary sectors, additional allocation of water resources to these sectors can effectively reduce the rate of water scarcity and increase the efficiency of water supply, thus improving the overall robustness of the system. The overall improvement in the robustness of the system will be achieved.

In the UMHR region, water supply for domestic use and the secondary and tertiary sectors is a key factor influencing the spatial equilibrium robustness of water allocation while respecting the individual needs of each geospatial and water-using sector. By prioritizing the supply of water for domestic use as well as for secondary and tertiary industries, not only can the spatial equilibrium robustness of water

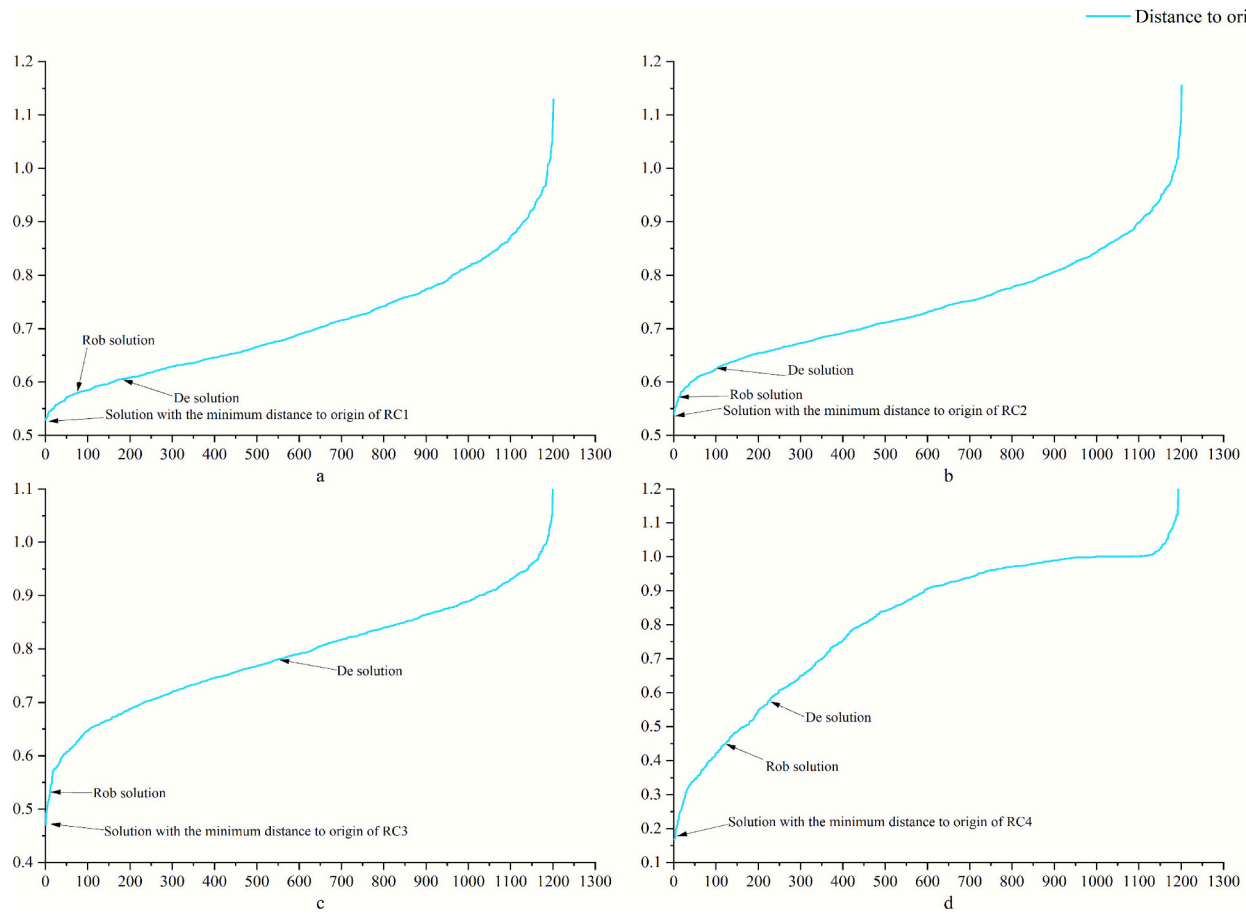

Fig. 16. 1201 solutions on the combined robustness performance of the four robustness metrics (a:RC1, b:RC2, c:RC3, d:RC4).

allocation be improved, but it can also help to reduce the rate of water scarcity and pollutant discharge, thus achieving a better robustness performance in the three objective functions. This finding provides an essential theoretical basis and practical guidance for water resources management and policy-making in the Huaihe River Basin and other regions and emphasizes the need to comprehensively consider the demands of different water-using sectors and their impacts on the overall water resources management objectives in formulating water resources allocation strategies.

4.8. Comparison of spatial equilibrium model robust solutions and traditional model robust solutions

As shown in Table 6, the performance of the spatial equilibrium model integrated robust solution with the traditional model integrated robust solution in terms of spatial equilibrium is analyzed, especially in the two key indexes of the Gini coefficient and the water deficit rate. The results show that the spatial equilibrium model composite robust solution significantly outperforms the traditional model robust solution in improving the spatial equity of water allocation and reducing the risk of water deficit. Specifically, the average value of the Gini coefficient of the traditional model integrated robust solution is 0.25. In contrast, the average value of the Gini coefficient of the spatial equilibrium model integrated robust solution is only 0.0998, which clearly shows that the spatial equilibrium model integrated robust solution has a significant advantage in improving the spatial equilibrium of water resources allocation. In addition, analyzing from the perspective of water deficit rate, the average value of water deficit rate of the spatial equilibrium model integrated robust solution is 0.8, compared with the average value of water deficit rate of the traditional model integrated robust solution of 1.31, which further confirms the superiority of the spatial equilibrium model integrated robust solution in terms of the robustness of water deficit rate.

However, when the objective of pollutant emissions is taken into account, the spatial equilibrium model composite robust solution does not perform as robustly as the traditional model composite robust solution. This difference may be closely related to the objective function setting and water allocation scheme adopted by the two models. The spatial equilibrium model is designed to pay more attention to the fairness of water allocation and the minimization of water scarcity risk, which may be sacrificed to some extent to the concern of pollutant emission control.

Therefore, water resources management strategies in the HRB and other regions should take into account multiple factors, including spatial balance, water scarcity rate, and environmental impacts. Decision makers should also pay attention to controlling pollutant emissions while pursuing spatial equilibrium and the robustness of the water scarcity rate to realize the comprehensive sustainability of water resources management. Comparison of the two model solutions demonstrates that the spatial equilibrium model not only enhances the equity of water allocation and reduces the risk of water deficit but also highlights the need to balance environmental and socio-economic factors to achieve sustainable water management objectives.

Although the traditional model emphasizes social harmony, stability, and environment protection, its tendency to prioritize domestic and secondary and tertiary sectors in water supply may result in insufficient allocation to agriculture sector due to the higher allocation benefit and lower discharge characteristics of these sectors. This bias contrasts with the “spatial equilibrium” definition proposed here: “respecting the individual development needs of each region and ensuring the equity and

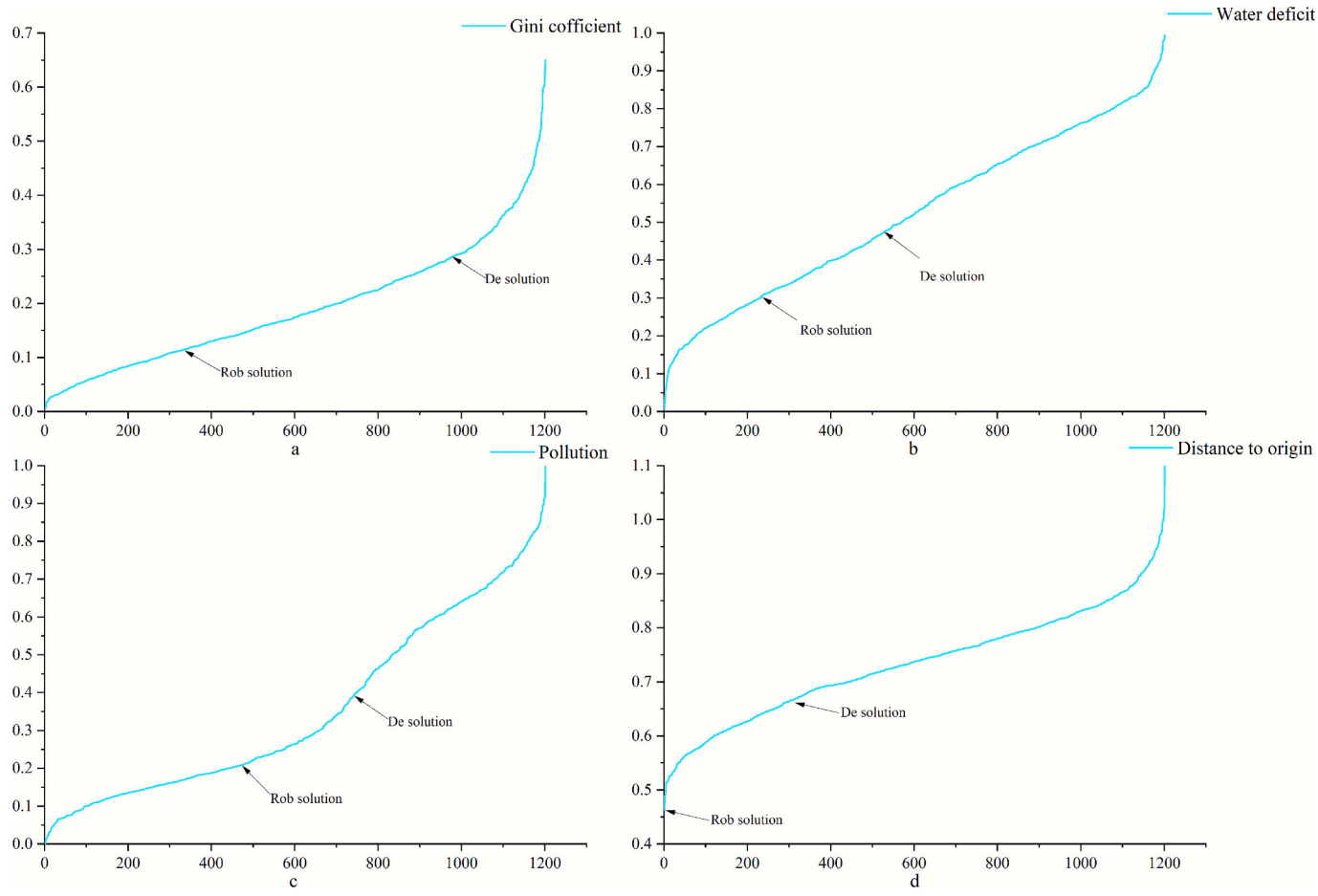

Fig. 17. Combined robustness performance of 1201 solutions.

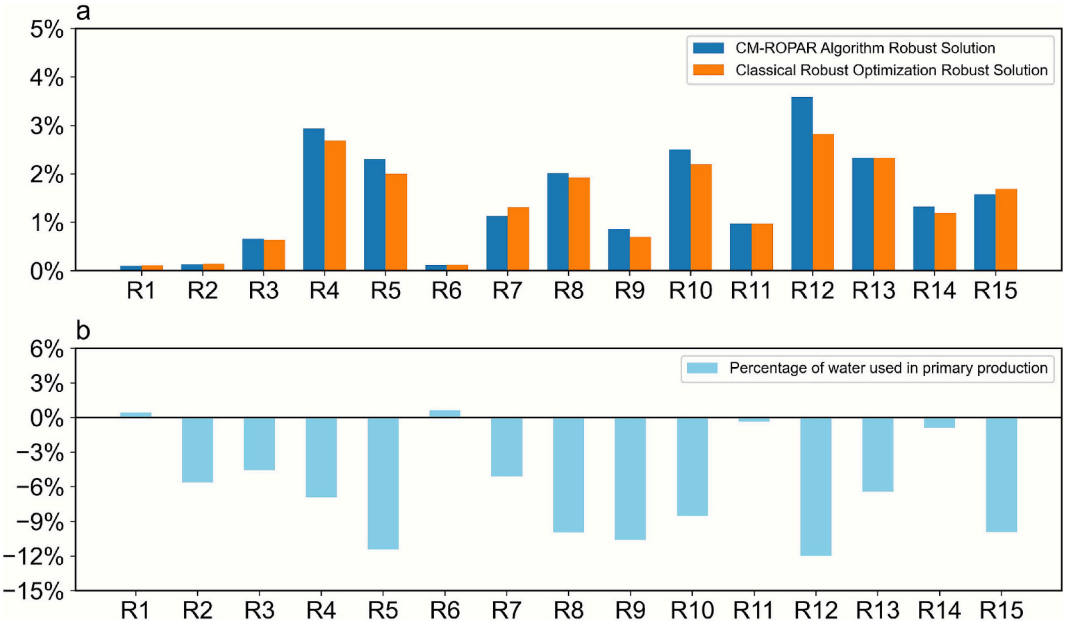

Fig. 18. Comparison of spatially equilibrated robust and deterministic allocation schemes. The horizontal axis represents region codes. The vertical axis in Fig. 18(a) indicates the proportion of allocated water volume for each region. The vertical axis in Fig. 18(b) indicates the difference between the agricultural water supply proportion from the RMOMC Algorithm Robust Solution and that from the Classical Robust Optimization Robust Solution.

Table 6
Comparison of robustness of spatial equilibrium model robust solutions and traditional model robust solutions.

Configuration options	objective function	*RC*1	*RC*2	*RC*3	*RC*4
Comprehensive robust solutions for spatial equilibrium models	Gini coefficient	0.098	0.101	1.995E-04	0.00 %
	Total water deficit	0.80	1.55	0.05	13.67 %
	Pollution emissions	27626.98	32759.43	1598.89	40.67 %
Traditional model robust solution	Gini coefficient	0.251	0.277	1.71E-03	100.00 %
	Total water deficit	1.31	1.90	0.17	88.00 %
	Pollution emissions	25318.92	29922.58	1465.31	0.00 %

Fig. 19. Comparison of spatial equilibrium model robust solution and traditional model robust solution allocation schemes. The horizontal axis represents region codes. The vertical axis in Fig. 19(a) indicates the proportion of allocated water volume for each region. The vertical axis in Fig. 19(b) indicates the difference between the agricultural water supply proportion from the comprehensive robust allocation scheme of the spatial equilibrium model and that from the traditional model's comprehensive robust allocation scheme.

coordination of water allocation". This limitation of the traditional model ignores the importance of food production and violates the principle of spatially balanced allocation that integrates population, agricultural water demand, and GDP.

Comparing the water supply shares of the two water allocation scenarios, as shown in Fig. 19(a), the spatial equilibrium model integrated robustness scenario increases the water supply to the upstream R4 and R5, R10, R12, R13, and R14. Among them, the water supply shares of R12 and R10 are especially increased because the water demands of R12, R5, and R10 are the three cities with the highest water demand, which can be 12.43 %, 11.36 %, and 11.23 %, and the increase of water supply to these three cities can be a good solution. The water demand of R12 can be up to 12.43 %, R5 can be up to 11.36 %, and R10 can be up to 11.23 %, so increasing the water supply to these three cities can improve the spatial balance.

Specifically for the water use sector, the spatial equilibrium model's agricultural water use increases substantially while the domestic water use remains stable for both models' robustness scenarios. As shown in Fig. 19(b), similar to the previous section, positive values indicate that the spatial equilibrium model integrated robustness allocation solution accounts for a larger share of agricultural water supply than the traditional model integrated robustness allocation solution, and negative values indicate that agricultural water supply accounts for a smaller share. It is evident from Fig. 19 that the spatial equilibrium model robust solution significantly increases agrarian water supply, with 11 out of 15 regions getting a significant increase in agricultural water supply. This shows that compared with the traditional model, the spatial equilibrium model can better consider the various water-using sectors without favoring the sectors with high unilateral water efficiency to achieve the balanced development of different regions and sectors.

The findings highlight the importance of achieving spatial equilibrium in water resources management while pointing out the contribution of multidimensional factors, including respecting the water demand of various sectors, enhancing agricultural water availability, and accounting for water source availability and spatial heterogeneity, to achieving a balanced, coordinated, and sustainable allocation of water resources in the region. These findings have important theoretical and practical implications for developing more scientific, equitable, and sustainable water resources management strategies.

5. Conclusion

Addressing the current water resources allocation research dominated by deterministic models and focused on economic development, this study develops a spatial equity-oriented optimization framework that jointly accounts for socioeconomic and ecological objectives, aligns allocation with regional needs, and reduces interregional disparities. In view of the heightened uncertainty in hydrologic variables driven by climate change and human activities, this study further introduces a new robust optimization approach that assesses allocation robustness across multiple dimensions and scenarios.

At methodological level, this study proposes a composite Gini coefficient for water resources alongside GDP, population, and agricultural water demand as one of the objective functions to measure the spatial

equilibrium of water resource allocation. The R-Vine Copula function is employed to analyze the wet-dry encounter patterns between the mainstem and tributary inflows within the basin. The RMOMC algorithm is proposed to explicitly demonstrate the propagation patterns of uncertainty factors, enabling multidimensional assessment of allocation scheme robustness and identification of the optimal solution with the highest comprehensive robustness.

At the application level, this study focuses on the middle and upper reaches of the Huai River basin. Research indicates that the scenario where the main stream and four tributary sections exhibit identical wet and dry conditions has the highest probability, with respective probabilities of 2.55 %, 7.85 %, and 3.28 % for wet, normal, and dry years. The proposed spatially balanced allocation scheme achieves a comprehensive Gini coefficient below 0.2, indicating spatial equilibrium. The water scarcity rate is 19.24 %, representing a 45.42 % reduction compared with the classical water resource allocation scheme. Compared with the classical robust optimization algorithm, the robustness of the allocation scheme improves by 45.3 %.

This research still has some limitations. In the field of reservoir cluster optimization scheduling, some scholars have considered the sensitivity of objective functions across different scheduling periods. They have constructed a multi-objective optimization scheduling model for reservoir clusters that accounts for the time-varying scheduling preferences of managers (Ni et al., 2022), thereby enhancing the alignment between the mathematical model and real-world conditions. The water resource allocation model in this study assumes that water resources managers' preferences for allocation objectives remain constant and uniform throughout the year, which deviates from real-world conditions. Therefore, future research will introduce robust assessment models and water resource optimization allocation models incorporating time-varying preferences to better align with the demands of practical water resource management.

CRediT authorship contribution statement

Jitao Zhang: Formal analysis, Conceptualization. **Jinyu Meng:** Writing – original draft, Software. **Zengchuan Dong:** Writing – review & editing, Supervision. **Dimitri Solomatine:** Writing – review & editing, Methodology. **Hui Xu:** Methodology, Data curation. **Wenzhuo Wang:** Visualization, Data curation. **Daoli Wang:** Validation, Software. **Tianyan Zhang:** Writing – original draft, Data curation. **Guang Yang:** Validation, Methodology.

Declaration of competing interest

The authors declare that they have no known competing financial interests or personal relationships that could have appeared to influence the work reported in this paper.

Acknowledgements

The authors are grateful to the Huaihe River Basin Management Committee for providing valuable economic and hydrological data. The authors are also grateful to the insight and views of the reviewers and editors. This study is funded by National Natural Science Foundation of China Youth Science Fund Project (52509015) and National Natural Science Foundation of China Youth Science Fund Project (52309029).

Appendix A. Supplementary data

Supplementary data to this article can be found online at https://doi.org/10.1016/j.jhydrol.2025.134690.

Data availability

Data will be made available on request.

References

Abdulbaki, D., Al-Hindi, M., Yassine, A., et al., 2017. An optimization model for the allocation of water resources. J. Clean. Prod. 164, 994–1006.
Afzal, J., Noble David, H., Weatherhead, E.K., 1992. Optimization model for alternative use of different quality irrigation waters. J. Irrig. Drain. Eng. 118 (2), 218–228.
Blank, J., Deb, K., Roy, P.C., 2019. Investigating the Normalization Procedure of NSGA-III; proceedings of the Evolutionary Multi-Criterion Optimization, Cham, Springer International Publishing.
Cai, X., Mckinney Daene, C., Lasdon Leon, S., 2003. Integrated hydrologic-agronomic-economic model for river basin management. J. Water Resour. Plan. Manag. 129 (1), 4–17.
Candido Laíse, A., Coêlho Gabriella Autran, G., De Moraes Márcia Maria Guedes, A., et al., 2022. Review of decision support systems and allocation models for integrated water resources management focusing on joint water quantity-quality. J. Water Resour. Plan. Manag. 148 (2), 03121001.
Chakraei, I., Safavi Hamid, R., Dandy Graeme, C., et al., 2021. Integrated simulation-optimization framework for water allocation based on sustainability of surface water and groundwater resources. J. Water Resour. Plan. Manag. 147 (3), 05021001.
Copca Maya, E.O., Fuentes Mariles, Ó.A., 2025. Trivariate frequency analysis using copulas emphasizing the importance of the duration of hydrographs for hydraulic works. Hydrol. Res. 56 (8), 672–697.
Dai, T., Labadie, John W., 2001. River basin network model for integrated water quantity/quality management. J. Water Resour. Plan. Manag. 127 (5), 295–305.
Davidsen, C., Pereira-Cardenal Silvio, J., Liu, S., et al., 2015. Using stochastic dynamic programming to support water resources management in the Ziya River Basin, China. J. Water Resour. Plan. Manag. 141 (7), 04014086.
Deb, K., Pratap, A., Agarwal, S., et al., 2002. A fast and elitist multiobjective genetic algorithm: NSGA-II. IEEE Trans. Evol. Comput. 6 (2), 182–197.
Gorelick, S.M., Zheng, C., 2015. Global change and the groundwater management challenge. Water Resour. Res. 51 (5), 3031–3051.
Ji, P., Su, R., Wu, G., et al., 2025. Projecting future wetland dynamics under climate change and land use pressure: a machine learning approach using remote sensing and Markov chain modeling. Remote Sens. (Basel) 17 (6), 1089.
Jia, Y., Wang, H., Zhou, Z., et al., 2006. Development of the WEP-L distributed hydrological model and dynamic assessment of water resources in the Yellow River basin. J. Hydrol. 331 (3), 606–629.
Kaya, Y., 2025. Evaluation of ICESat-2 laser altimetry for inland water level monitoring: a case study of Canadian Lakes. Water 17 (7), 1098.
Kaya, Y., 2025. Slope-aware and self-adaptive forecasting of water levels: a transparent model for the Great Lakes under climate variability. J. Hydrol. 662, 133948.
Khosravi, K., Farooque, A.A., Karbasi, M., et al., 2025. Enhanced water quality prediction model using advanced hybridized resampling alternating tree-based and deep learning algorithms. Environ. Sci. Pollut. Res. 32 (11), 6405–6424.
Küçükoğlu, M., Kaya, Y., 2026. Global evolution of inland water levels: drying-speed analysis using ICESat-2 ATL13. J. Hydrol. 664, 134486.
Kumar, V., Yadav, S.M., 2022. A state-of-the-Art review of heuristic and metaheuristic optimization techniques for the management of water resources. Water Supply 22 (4), 3702–3728.
Li, M., Fu, Q., Singh, V.P., et al., 2018. An interval multi-objective programming model for irrigation water allocation under uncertainty. Agric. Water Manag. 196, 24–36.
Li, Y.P., Huang, G.H., Huang, Y.F., et al., 2009. A multistage fuzzy-stochastic programming model for supporting sustainable water-resources allocation and management. Environ. Model. Software 24 (7), 786–797.
Li, B.-J., Sun, G.-L., Liu, Y., et al., 2022. Monthly runoff forecasting using variational mode decomposition coupled with gray wolf optimizer-based long short-term memory neural networks. Water Resour. Manag. 36 (6), 2095–2115.
Li, D., Zuo, Q., Jiang, L., et al., 2023. An integrated analysis framework for water resources sustainability considering fairness and decoupling based on the water resources ecological footprint model: a case study of Xinjiang, China. J. Clean. Prod. 383, 135466.
Liu, J., Tian, Y., Huang, K., et al., 2021. Spatial-temporal differentiation of the coupling coordinated development of regional energy-economy-ecology system: a case study of the Yangtze River Economic Belt. Ecol. Ind. 124, 107394.
Lu, B., Li, K., Zhang, H., et al., 2013. Study on the optimal hydropower generation of Zhelin reservoir. J. Hydro Environ. Res. 7 (4), 270–278.
Madani, K., 2010. Game theory and water resources. J. Hydrol. 381 (3), 225–238.
Meraj, G., Hashimoto, S., 2025. Bridging the adaptation finance gap: the role of nature-based solutions for climate resilience. Sustain. Sci. 20 (3), 1093–1107.
Naderi, M.M., Mirchi, A., Bavani, A.R.M., et al., 2021. System dynamics simulation of regional water supply and demand using a food-energy-water nexus approach: Application to Qazvin Plain, Iran. J. Environ. Manage. 280, 111843.
Ni, X., Dong, Z., Jiang, Y., et al., 2022. A subjective-objective integrated multi-objective decision-making method for reservoir operation featuring trade-offs among non-inferior solutions themselves. J. Hydrol. 613, 128430.
O'Connell, E., 2017. Towards adaptation of water resource systems to climatic and socio-economic change. Water Resour. Manag. 31 (10), 2965–2984.
Pan, Z., Yang, S., Lou, H., et al., 2023. Perspectives of human–water co-evolution of blue–green water resources in subtropical areas. Hydrol. Process. 37 (2), e14818.
Qi, P., Sun, J., Zhang, G., 2025. Optimal allocation of water and land resources considering crop water demand process from the perspective of water-carbon-economy nexus. J. Hydrol. 654, 132831.
Qu, B., Jiang, E., Li, J., et al., 2024. Coupling coordination relationship of water resources, eco-environment and socio-economy in the water-receiving area of the lower Yellow River. Ecol. Ind. 160, 111766.

Shuai, Y., He, X., Yao, L., 2022. Robust optimization with equity and efficiency framework for basin-wide water resources planning. J. Environ. Manage. 321, 115834.
Sun, S., Wang, Y., Liu, J., et al., 2016. Sustainability assessment of regional water resources under the DPSIR framework. J. Hydrol. 532, 140–148.
Tian, J., Guo, S., Liu, D., et al., 2019. A fair approach for multi-objective water resources allocation. Water Resour. Manag. 33 (10), 3633–3653.
Unami, K., Mohawesh, O., Fadhil, R.M., 2019. Time periodic optimal policy for operation of a water storage tank using the dynamic programming approach. Appl. Math Comput. 353, 418–431.
Vališ, D., Hasilová, K., Forbelská, M., et al., 2020. Reliability modelling and analysis of water distribution network based on backpropagation recursive processes with real field data. Measurement 149, 107026.
Wang, W., Dong, Z., Lall, U., et al., 2019. Monthly streamflow simulation for the headwater catchment of the Yellow River basin with a hybrid statistical-dynamical model. Water Resour. Res. 55 (9), 7606–7621.
Wang, T., You, J., Ma, Z., et al., 2022. A hierarchical index system for analysis of water supply-demand situation. Water Resour. Manag. 36 (12), 4485–4498.
Wu, J., Wang, Z., Hu, Y., et al., 2023. Runoff forecasting using convolutional neural networks and optimized bi-directional long short-term memory. Water Resour. Manag. 37 (2), 937–953.
Yuan, M., Zheng, N., Yang, Y., et al., 2023. Robust optimization for sustainable agricultural management of the water-land-food nexus under uncertainty. J. Clean. Prod. 403, 136846.
Zhang, L., Feng, Z.-K., Yao, X.-R., et al., 2024. A multi-objective operation optimization method for dynamic control of reservoir water level in evolving flood season environments. J. Hydrol. 643, 131940.
Zhang, C., Li, X., Guo, P., et al., 2022. Enhancing irrigation water productivity and controlling salinity under uncertainty: a full fuzzy dependent linear fractional programming approach. J. Hydrol. 606, 127428.
Zhang, J., Solomatine, D., Dong, Z., 2024. Robust multi-objective optimization under multiple uncertainties using the CM-ROPAR approach: case study of water resources allocation in the Huaihe River basin. Hydrol. Earth Syst. Sci. 28 (16), 3739–3753.
Zhang, F., Wu, Z., Di, D., et al., 2023. Water resources allocation based on water resources supply-demand forecast and comprehensive values of water resources. J. Hydrol.: Reg. Stud. 47, 101421.
Zhang, Z., Zhang, J., Guan, Q., et al., 2025. Multi-objective optimal allocation and spatial distribution of water and land resources in Yellow River Basin irrigated farmland: a government-farmer duality perspective. J. Hydrol. 662, 134070.
Zhu, K., Qiu, X., Luo, Y., et al., 2022. Spatial and temporal dynamics of water resources in typical ecosystems of the Dongjiang River Basin, China. J. Hydrol. 614, 128617.